

Forecasting in Offline Reinforcement Learning for Non-stationary Environments

Suzan Ece Ada^{1,2} Georg Martius² Emre Ugur¹ Erhan Oztop^{3,4}
¹Bogazici University, Türkiye ²University of Tübingen, Germany
³Ozyegin University, Türkiye ⁴Osaka University, Japan
 ece.ada@bogazici.edu.tr

Abstract

Offline Reinforcement Learning (RL) provides a promising avenue for training policies from pre-collected datasets when gathering additional interaction data is infeasible. However, existing offline RL methods often assume stationarity or only consider synthetic perturbations at test time, assumptions that often fail in real-world scenarios characterized by abrupt, time-varying offsets. These offsets can lead to partial observability, causing agents to misperceive their true state and degrade performance. To overcome this challenge, we introduce **Forecasting in Non-stationary Offline RL (FORL)**, a framework that unifies (i) conditional diffusion-based candidate state generation, trained without presupposing any specific pattern of future non-stationarity, and (ii) zero-shot time-series foundation models. FORL targets environments prone to unexpected, potentially non-Markovian offsets, requiring robust agent performance from the onset of each episode. Empirical evaluations on offline RL benchmarks, augmented with real-world time-series data to simulate realistic non-stationarity, demonstrate that FORL consistently improves performance compared to competitive baselines. By integrating zero-shot forecasting with the agent’s experience, we aim to bridge the gap between offline RL and the complexities of real-world, non-stationary environments.

1 Introduction

Offline Reinforcement Learning (RL) leverages static datasets to avoid costly or risky online interactions [1, 2]. Yet, agents trained on fully observable states often fail when deployed with noisy or corrupted observations. While robust offline RL methods address test-time perturbations, such as sensor noise or adversarial attacks [3], a critical gap persists in addressing non-stationarity within the observation function—a challenge that fundamentally alters the agent’s perception of the environment over time.

Prior *online algorithms* that consider the scope of non-stationarity as the observation function focus on learning agent morphologies [4] and generalization in Block MDPs [5]. While this scope of non-stationarity holds significant potential for real-world applications [6], it remains underexplored. We focus on the episodic evolution of the observation function at test-time in offline RL. In our setup, each dimen-

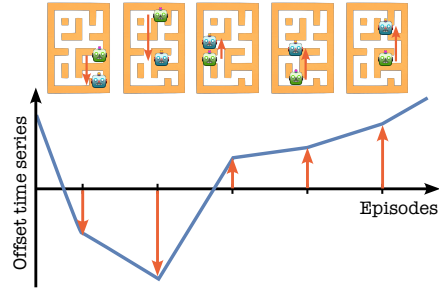


Figure 1: **Setting.** The agent does not know its location in the environment because its perception is offset every episode j by an unknown offset b^j (only vertical offsets are illustrated). FORL leverages historical offset data and offline RL data (from a stationary phase) to forecast and correct for new offsets at test time. Ground-truth offsets (\downarrow, \uparrow) are hidden throughout the evaluation episodes.

sion of an agent’s state is influenced by an unknown, time-dependent constant additive offset that remains fixed within a single operational interval (an “episode”). This leads to a stream of evolving observation functions [7], extending across multiple future episodes, **where the offsets remain hidden throughout the prediction window**. For instance, industrial robots might apply a daily calibration offset to each joint, while sensors can exhibit a deviation until the next scheduled recalibration. Similarly, in healthcare or finance, data may be partially aggregated or withheld to comply with regulations, effectively obscuring finer-grained variations and leaving a single offset as the dominant factor per episode. By only storing these representative offsets, we circumvent the challenges of continuous interaction buffers in bandwidth-constrained or privacy-sensitive environments. Because the offset can differ across state dimensions (e.g., different sensor or actuation channels), each state dimension can be affected by a different unknown bias that stays constant for that episode but evolves differently across episodes. Approaches that assume predefined perturbations can struggle with these abrupt, episodic shifts, because such offsets violate the typical assumption of smoothly varying observation functions. Frequent retraining, hyperparameter optimization, or extensive online adaptation to new observation function evolution patterns are costly, risky (due to trial-and-error in safety-critical settings), and may be infeasible if these patterns no longer reflect assumptions made during training. By separating offset data (episodic calibration values) from the massive replay buffers, a zero-shot forecasting-based approach can anticipate each new offset from the beginning of the episode without requiring policy updates or making assumptions on task evolution at test time [8]. Modeling these multidimensional additive offsets as stable, per-episode constants presents a robust and efficient way to handle time-varying conditions in non-stationary environments where the evolution of tasks follows a non-Markovian, time-series pattern [9], mitigating the risks of online exploration.

We consider an offline RL setting during training where we have only access to a standard offline RL dataset collected from a stationary environment [3] with fully observable states. Initial data may be collected under near-ideal conditions and then gradually affected by wear, tear, or other natural shifts—even as the underlying physical laws (dynamics) remain unchanged. At test time, however, we evaluate in a non-stationary environment where both the observation function and the observation space change due to time-dependent external factors. This setup can be interpreted as environments shifting along observation space dimensions while the initial state of the agent is sampled from a uniform distribution over the state space. A simplified version of this setup for an offset affecting only one dimension of the state is illustrated in Figure 1. Here, the agent “knows” it is in a maze but does not know where it is in the maze. Furthermore, **it will remain uncertain of its location across all episodes at test-time**, as in every episode, a new offset leads to a systematic misalignment between perceived and actual positions. Importantly, these offsets may not conform to Gaussian or Markovian assumptions; instead, they may stem directly from complex, real-world time-series data [9] and remain constant throughout each episode. As a result, standard noise-driven or parametric state-estimation techniques, which typically rely on smoothly varying or randomly perturbed functions, cannot reliably identify these persistent, episode-wide offsets that are not available after the episode terminates. While zero-shot forecasting can adjust observation offsets, its performance depends on the forecaster’s accuracy. Similarly, integrating zero-shot forecasting into a model-based offline RL approach [3] can underperform when real-world offsets deviate from predefined assumptions about future observation functions. Our approach uses the insight that the belief of the true states can be refined from a sequence of actions and effects. For instance, in maze navigation, if an agent misjudges its location and hits a wall, analyzing its actions and delta observations leading to the collision can provide evidence for likely locations within the maze.

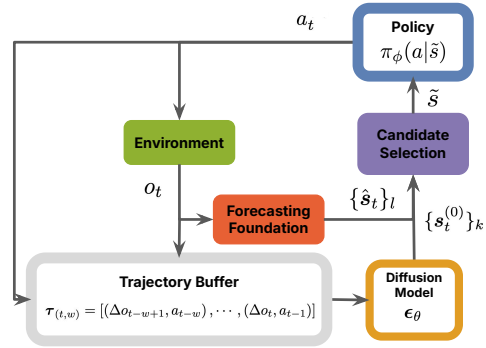


Figure 2: Overview of the proposed FORL framework at test-time. The observations are processed by both the trajectory buffer and the time-series **forecasting foundation** module [10]. Observation changes and actions sampled from the **policy** ($\Delta o, a$), are stored in the trajectory buffer. The **diffusion model** generates candidate states $\{s_t^{(0)}\}_k$ conditioned on $\tau_{(t,w)}$. The **candidate selection** module then generates the estimated \tilde{s}_t .

We propose the **Forecasting in Non-stationary Offline RL (FORL)** framework (Figure 2) for test-time adaptation in non-stationary environments where the observation function is perturbed by an arbitrary time-series. Our framework has two main ingredients: forecasting offsets with a zero-shot time-series forecasting model [10] from past episode offsets (ground truth offsets after the episode terminates are not accessible at test-time) and a within-episode update of the state estimation using a conditional diffusion model [11] trained on offline stationary data.

Contributions. We unify the strengths of probabilistic forecasting and decision-making under uncertainty to enable continuous adaptation when the environment diverges from predictions. Consequently, our framework: (1) accommodates future offsets *without assuming specific non-stationarity patterns during training*, eliminating the need for retraining and hyperparameter tuning when the agent encounters new, unseen non-stationary patterns at test time, and (2) *targets non-trivial non-stationarities at test time without requiring environment interaction or knowledge of POMDPs during training*. (3) FORL introduces a novel, modular framework combining a conditional diffusion model (FORL-DM) for multimodal belief generation with a lightweight Dimension-wise Closest Match (DCM) fusion strategy, validated by extensive experiments on no-access to past offsets, policy-agnostic plug-and-play, offset magnitude-scaling, and inter/intra-episode drifts. (4) We propose a novel benchmark that integrates offsets from real-world time-series datasets with standard offline RL benchmarks and demonstrate that FORL consistently outperforms baseline methods.

Background: Diffusion Models Denoising diffusion models [12, 13] aim to model the data distribution with $p_\theta(\mathbf{x}_0) := \int p_\theta(\mathbf{x}_{0:N}) d\mathbf{x}_{1:N}$ from samples \mathbf{x}_0 in the dataset. The joint distribution follows the Markov Chain $p_\theta(\mathbf{x}_{0:N}) := \mathcal{N}(\mathbf{x}_N; \mathbf{0}, \mathbf{I}) \prod_{n=1}^N p_\theta(\mathbf{x}_{n-1} | \mathbf{x}_n)$ where \mathbf{x}_n is the noisy sample for diffusion timestep n and $p_\theta(\mathbf{x}_{n-1} | \mathbf{x}_n) := \mathcal{N}(\mathbf{x}_{n-1}; \boldsymbol{\mu}_\theta(\mathbf{x}_n, n), \boldsymbol{\Sigma}_\theta(\mathbf{x}_n, n))$. During training, we use the samples from the distribution $q(\mathbf{x}_n | \mathbf{x}_0) = \mathcal{N}(\mathbf{x}_n; \sqrt{\bar{\alpha}_n}\mathbf{x}_0, (1 - \bar{\alpha}_n)\mathbf{I})$ where $\bar{\alpha}_n = \prod_{i=1}^n \alpha_i$ [11]. General information on diffusion models is given in Section B.3.

2 Method

In this section, we formulate our problem statement and describe our FORL diffusion model trained on the offline RL dataset to predict plausible states. Then, we introduce our online state estimation method, Dimension-wise Closest Match that uses plausible states predicted by the multimodal FORL diffusion model (DM) and the states predicted from past episodes prior to evaluation by a probabilistic unimodal zero-shot time-series foundation model.

2.1 Problem Statement

Training (Offline Stationary MDP) We begin with an episodic, stationary Markov Decision Process (MDP) $\mathcal{M}_{\text{train}} = (\mathcal{S}, \mathcal{A}, \mathcal{T}, \mathcal{R}, \rho_0)$, where the initial state distribution ρ_0 is a uniform distribution over the state space \mathcal{S} . We only have access to an offline RL dataset $\mathcal{D} = \{(\mathbf{s}_t^k, \mathbf{a}_t^k, \mathbf{s}_{t+1}^k, r_t^k)\}$ with k transitions collected from this MDP. Crucially, our FORL diffusion model and a diffusion policy [14] are trained offline using this dataset, such as the standard D4RL benchmark [15], without making any assumptions about how the environment might become non-stationary at test time.

Test Environment (Sequence of POMDPs) At test time, the agent faces an infinite sequence of POMDPs $\{\hat{\mathcal{M}}_j\}_{j=1}^\infty$. Each POMDP is described by a 7-tuple [16] $\hat{\mathcal{M}}_j = (\mathcal{S}, \mathcal{A}, \mathcal{O}_j, \mathcal{T}, \mathcal{R}, \rho_0, \mathbf{x}_j)$, where the state space \mathcal{S} , action space \mathcal{A} , transition function \mathcal{T} , and the reward function \mathcal{R} remain identical to the training MDP. \mathbf{x} is the observation function, where we restrict ourselves to deterministic versions ($\mathbf{x} : \mathcal{S} \rightarrow \mathcal{O}$) [6, 17]. Non-stationary environments can be formulated in different ways. In Khetarpal et al. [6], a *general non-stationary RL* formulation is put forward, which allows each component of the underlying MDP or POMDP to evolve over time, i.e. $(\mathcal{S}(t), \mathcal{A}(t), \mathcal{T}(t), \mathcal{R}(t), \mathbf{x}(t), \mathcal{O}(t))$. A set κ specifies which of these components vary, and a *driver* determines how they evolve. In particular, *passive* drivers of non-stationarity imply that exogenous factors alone govern the evolution of the environment, independent of the agent’s actions. In this work, we consider the scope of non-stationarity [6] (Section B.2) to be the observation function and the observation space, i.e. $\kappa = \{\mathbf{x}, \mathcal{O}\}$.

We consider the case where non-stationarity unfolds over episodes and where the observation function \mathbf{x}_j is different in each episode j . The change in the observation function is assumed to have an

additive structure and is independent of the agent’s actions (passive non-stationarity [6]). Concretely, the function \mathbf{x}_j offsets states s_t by a fixed offset $b^j \in \mathbb{R}^n$:

$$\mathcal{O}_j = \{s + b^j : s \in \mathcal{S}\}, \quad \mathbf{x}_j(s) = s + b^j.$$

Importantly, the sequence (b^j) can evolve under arbitrary real-world time-series data, and the agent **does not have access to the ground-truth information throughout the evaluation**—similar to scenarios where observations are only available periodically and shifts occur between these intervals. Thus, the episodes have a temporal order, relating to Non-Stationary Decision Processes (NSDP), defining a sequence of POMDPs [7] (Section B.2).

Partial Observability and Historical Context Since b^j is **never directly observed** for P episodes into the future, each $\hat{\mathcal{M}}_j$ is a POMDP. The agent receives only the offset-shifted observations (o_t), where $o_t = s_t + b^j$ without any noise. Moreover, the agent may have access to a limited historical context of previous offsets $(b^{j-C}, \dots, b^{j-1})$ at discrete intervals P , but **no direct information** about future offsets $(b^j, b^{j+1}, \dots, b^{j+P-1})$. Hence, the agent must forecast and/or adapt to unknown future offsets without prior non-stationary training.

Partial Identifiability Despite observing $o_t = s_t + b^j$, the agent cannot generally disentangle s_t from b^j . For any single observation, there are infinite possible pairs of state and offset that yield $o_t = s' + b'$. Additionally, the initial state distribution ρ is uniform and does not provide information about b . Thus, we can only form a belief over s_t and refine that belief based on two sources of information: a) the sequence of actions and effects observed within an episode and b) the sequence of past identified offsets. To exploit source a, we utilize a predictive model of commonly expected outcomes based on a diffusion model, which will be explained next. To make use of source b, we use a zero-shot forecasting model (see Section 2.3 for details). Afterwards, both pieces of information are fused (Section 2.4).

2.2 FORL Diffusion Model

In our setting, we assume that the offsets added to the states are unobservable at test time, while the transition dynamics of the evaluation environment remain unchanged. To eventually reduce the uncertainty about the underlying state, we perform filtering or belief updates using the sequence of past interactions. To understand why the history of interactions is indicative of a particular ground truth state, consider the following example in a maze environment illustrated in Fig. 3. When the agent moves north for three steps and then bumps into a wall, the possible ground truth states can only be those three steps south of any wall. The agent cannot observe the hidden green trajectory of ground-truth states; it only has access to the sequence of observation changes (Δo) and action vectors, which narrows down the possible positions to four candidate regions—exactly those identified by our model. Clearly, the distribution of possible states is highly multimodal, such that we propose using a diffusion model as a flexible predictive model of plausible states given the observed actions and outcomes. Diffusion models excel at capturing multimodal distributions [14], making them well-suited for our task. We train the diffusion model on offline data without offsets ($b_j = 0$) which we detail below.

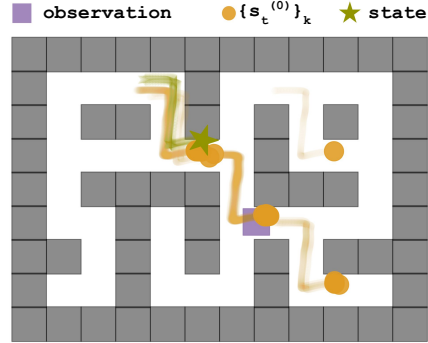


Figure 3: Candidate states generated by FORL Diffusion Model.

To distinguish between the trajectory timesteps in reinforcement learning (RL) and the timesteps in the diffusion process, we use the subscript $t \in \{0, \dots, T\}$ to refer to RL timesteps and $n \in \{0, \dots, N\}$ for diffusion timesteps. We first begin by defining a subsequence of a trajectory

$$\tau_{(t,w)} = [(\Delta o_{t-w+1}, a_{t-w}), \dots, (\Delta o_t, a_{t-1})]. \quad (1)$$

where delta observations $\Delta o_t = o_t - o_{t-1} = s_t - s_{t-1}$ denote the state changes (effects), w is the window size. Using a conditional diffusion model, we aim to model the distribution $p(s_t | \tau_{(t,w)})$. For that, we define the reverse process (denoising) as

$$p(s_t^{(N)}) \prod_{n=1}^N p_\theta(s_t^{(n-1)} | s_t^{(n)}, \tau_{(t,w)}), \quad p(s_t^{(N)}) = \mathcal{N}(s_t^{(N)}; \mathbf{0}, \mathbf{I}) \quad (2)$$

and p_θ is modeled as the distribution $\mathcal{N}(\mathbf{s}_t^{(n-1)}; \mu_\theta(\mathbf{s}_t^{(n)}, \boldsymbol{\tau}_{(t,w)}, n), \Sigma_\theta(\mathbf{s}_t^{(n)}, \boldsymbol{\tau}_{(t,w)}, n))$ with a learnable mean and variance. We could directly supervise the training of μ_θ using the forward (diffusion) process. Following Ho et al. [11], Song et al. [18], we compute a noisy sample $\mathbf{s}_t^{(n)}$ based on the true sample $\mathbf{s}_t = \mathbf{s}_t^{(0)}$:

$$\mathbf{s}_t^{(n)} = \sqrt{\bar{\alpha}(n)}\mathbf{s}_t + \sqrt{1 - \bar{\alpha}(n)}\boldsymbol{\epsilon} \quad (3)$$

where $\boldsymbol{\epsilon} \sim \mathcal{N}(\mathbf{0}, \mathbf{I})$ is the noise, $\bar{\alpha}(n) = \prod_{i=1}^n \alpha(i)$ and the weighting factors $\alpha(n) = e^{-(\beta_{\min}(\frac{1}{N}) + (\beta_{\max} - \beta_{\min})\frac{2n-1}{2N^2})}$ where $\beta_{\max} = 10$ and $\beta_{\min} = 0.1$ are parameters introduced for empirical reasons [19].

We can equally learn to predict the true samples by learning a noise model [20]. Hence, we train a noise model $\epsilon_\theta(\mathbf{s}_t^{(n)}, \boldsymbol{\tau}_{(t,w)}, n)$ that learns to predict the noise vector $\boldsymbol{\epsilon}$. By using the conditional version of the simplified surrogate objective from [11], we minimize

$$\mathcal{L}_p(\theta) = \mathbb{E}_{n, \boldsymbol{\tau}, \mathbf{s}_t, \boldsymbol{\epsilon}} \left[\left\| \boldsymbol{\epsilon} - \epsilon_\theta(\mathbf{s}_t^{(n)}, \boldsymbol{\tau}_{(t,w)}, n) \right\|^2 \right] \quad (4)$$

where \mathbf{s}_t is the state sampled from the dataset D for $t \sim U_T(\{w, \dots, T-1\})$, $\mathbf{s}_t^{(n)}$ is computed according to Eq. (3), $\boldsymbol{\epsilon}$ is the noise, and $n \sim U_D(\{1, \dots, N\})$ is the uniform distribution used for sampling the diffusion timestep.

We use the true data sample \mathbf{s}_t from the offline RL dataset to obtain the noisy sample in Eq. (3). Leveraging our model’s capacity to learn multimodal distributions, we generate a set of k samples $\{\mathbf{s}_t^{(0)}\}$ as our **predicted state candidates** in parallel from the reverse diffusion chain. We use the noise prediction model [11] with the reverse diffusion chain $\mathbf{s}_t^{(n-1)} | \mathbf{s}_t^{(n)}$ formulated as

$$\frac{\mathbf{s}_t^{(n)}}{\sqrt{\alpha(n)}} = \frac{1 - \alpha(n)}{\sqrt{\alpha(n)(1 - \bar{\alpha}(n))}} \epsilon_\theta(\mathbf{s}_t^{(n)}, \boldsymbol{\tau}_{(t,w)}, n) + \sqrt{1 - \alpha(n)}\boldsymbol{\epsilon} \quad (5)$$

where $\boldsymbol{\epsilon} \sim \mathcal{N}(\mathbf{0}, \mathbf{I})$ for $n = N, \dots, 1$, and $\boldsymbol{\epsilon} = \mathbf{0}$ for $n = 1$ [11]. Below, we detail how the state candidates are used during an episode.

2.3 Forecasting using Zero-Shot Foundation Model

Because we assume that the offsets b^j originate from a time series, we propose using a probabilistic zero-shot forecasting foundation model (*Zero-Shot FM*) such as Lag-Llama [10], to forecast future offsets from past ones. We assume that after P episodes, the true offsets are revealed, and we predict the offsets for the following P episodes. Using the probabilistic *Zero-Shot FM* we generate $(\hat{b}_l^j, \dots, \hat{b}_l^{j+P-1})$, where (l) denotes the number of samples generated for each episode (timestamp). Since Lag-Llama is a probabilistic model, it can generate multiple samples per timestamp, conditioned on C number of past contexts $(b^{j-C}, \dots, b^{j-1})$. In practice, we forecast every dimension of b independently since the *Zero-Shot FM* (Lag-Llama [10]) is a univariate probabilistic model.

2.4 FORL State Estimation

Algorithm 1 Candidate Selection

```

1: Sample  $\{\{\hat{b}_l^1, \dots, \hat{b}_l^P\} \sim \text{Zero-Shot FM}$ 
2: for each episode  $p = 1, \dots, P$  do
3:    $t = 0$ 
4:   Reset environment  $o_0 \sim \mathcal{E}$ 
5:    $\tilde{s} \leftarrow o_0 - \{\hat{b}_l^p\}$ 
6:   Initialize  $\boldsymbol{\tau}_{(t,w)}$ 
7:   while not done do
8:     Sample  $a^{(0)} \sim \pi_\phi(a|\tilde{s})$ 
9:     Take action  $a^{(0)}$  in  $\mathcal{E}$ , observe  $o_{t+1}$ 
10:     $\{\hat{s}_{t+1}^b\}_l \leftarrow o_{t+1} - \{\hat{b}_l^p\}$ 
11:     $\boldsymbol{\tau}_{(t+1,w)} = \text{PUSH}(\boldsymbol{\tau}_{(t,w)}, (\Delta o_{t+1}, a^{(0)}))$ 
12:     $\boldsymbol{\tau}_{(t+1,w)} = \text{POP}(\boldsymbol{\tau}_{(t+1,w)}, (\Delta o_{t-w+1}, a_{t-w}))$ 
13:    if  $t > w$  then
14:      Sample  $\{\mathbf{s}_{t+1}^{(0)}\}_k$  from FORL by Eq. 5
15:       $\tilde{s} \leftarrow \text{DCM}(\{\mathbf{s}_{t+1}^{(0)}\}_k, \{\hat{s}_{t+1}^b\}_l)$ 
16:    else
17:       $\tilde{s} \leftarrow o_{t+1} - \{\hat{b}_l^p\}$ 
18:    end if
19:     $t \leftarrow t + 1$ 
20:  end while
21: end for
```

The next step in our method is to fuse the information from the forecaster and the diffusion model into a state estimate used for control at test time.

At the beginning of an episode, no information can be obtained from the diffusion model, so for the first w steps we only rely on the forecaster’s mean prediction, i.e. $\tilde{s}_t = o_t - \hat{b}^j$ where the mean is taken over the l samples.

As soon as w steps are taken, our FORL *State Estimation* improves on the inferred state as detailed below. Figure 2 offers an overview of the entire system and Algorithm 1 provides a detailed pseudocode.

To recap, the diffusion model generates samples $\{s_t^{(0)}\}_k$ from the in-episode history τ , Eq. (1). These samples represent a multimodal distribution of plausible state regions. The *Zero-Shot FM* generates l samples of offsets $\{\hat{b}\}_l$ from which we compute forecasted states using $\{\hat{s}_t\}_l = o_t - \{\hat{b}\}_l$.

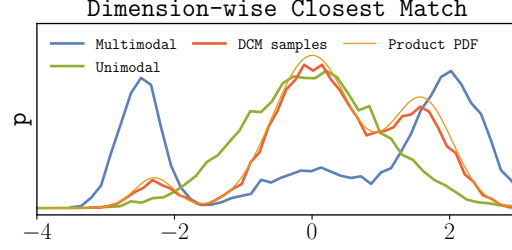


Figure 4: Distribution of samples produced by DCM (histograms for 10k samples for illustration).

FORL: Dimension-wise Closest Match (DCM) We propose a lightweight approach to sample a good estimate based on the samples from the multimodal (*diffusion model* $\{s_t^{(0)}\}_k$) and unimodal (*Zero-Shot FM* $\{\hat{s}_t^b\}_l$) distributions. Let $\mathcal{D}_{\text{diffusion}} = \{\mathbf{x}_1, \dots, \mathbf{x}_k\}$, $\mathcal{D}_{\text{timeseries}} = \{\mathbf{y}_1, \dots, \mathbf{y}_l\}$, where $\mathbf{x}_i, \mathbf{y}_j \in \mathbb{R}^n$. Then DCM constructs $\mathbf{z} \in \mathbb{R}^n$ by

$$z_d = y_{j^*(d),d} \quad \text{where} \quad j^*(d) = \arg \min_j \left(\min_i |x_{i,d} - y_{j,d}| \right),$$

where $d = 1 \dots n$. In other words, for each dimension d , we choose the sample from $\mathcal{D}_{\text{timeseries}}$ that has the closest sample in $\mathcal{D}_{\text{diffusion}}$. The process is straightforward yet effective, and under ideal sampling conditions for a toy dataset in Fig. 4, DCM approximately samples from the product distribution. DCM uses a non-parametric search to find the forecast sample with the highest score, which corresponds to the minimum dimension-wise distance. DCM’s prediction error is governed by the accuracy of the forecast samples in the unimodal $\mathcal{D}_{\text{timeseries}}$ that achieves this best score. As we will demonstrate in the experiments, this approach empirically yields lower maximum errors and is more stable compared to other methods.

FORL Algorithm Algorithm 1 summarizes the entire inference process at test time. We begin the episode by relying on the forecasted states \tilde{s}_0 . As more transitions $(\Delta o_t, a_{t-1})$ become available, the FORL diffusion model proposes candidate states $\{s_t^{(0)}\}_k$ through *retrospection*—reasoning over the past in-episode experience to adapt state estimation on the fly when they begin to diverge from predictions. We then invoke DCM to blend the diffusion model’s candidates with the foundation model’s unimodal forecasts and obtain the final state estimate \tilde{s}_t . We use an off-the-shelf offline RL policy such as Diffusion-QL (DQL) [14] to select the agent’s action a_t .

Summary By combining a powerful *zero-shot* forecasting model with a *conditional diffusion* mechanism, FORL addresses partial observability in continuous state and action space when ground-truth offsets are unavailable. This procedure is performed in the *absence of ground-truth offsets for past, current, and future episodes over the interval $j : j + P$ at test time*. DCM provides a computationally inexpensive yet effective way of using the multimodal diffusion candidates and unimodal time-series forecasts. This robust adaptation approach yields a state estimate \tilde{s}_t , aligned with the agent’s retrospective experience in the stationary offline RL dataset, incorporating a prospective external offset forecast.

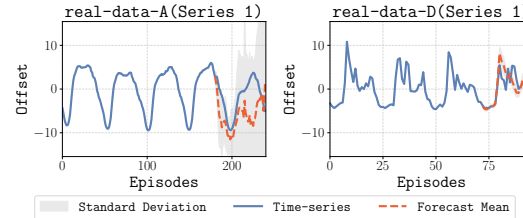


Figure 5: Zero-shot forecasting results of Lag-Llama [10] for the first univariate series (plotted from the real-data-A, D datasets; experiments use the **first two series from each dataset**).

3 Experiments

We evaluate FORL across navigation and manipulation tasks in D4RL [15] and OGBench [21] offline RL environments, each augmented with five real-world non-stationarity domains sourced from [22]. Fig. 5 presents the ground truth, forecast mean, and standard deviation from Lag-Llama [10] for the *first series* of real-data-A and real-data-D. Our experiments address the following questions: (1) Does FORL maintain state-of-the-art performance when confronted with unseen non-stationary offsets? (2) How can we use FORL when we have no access to delayed past ground truth offsets? (3) How does DCM compare to other fusion approaches? (4) Can FORL handle intra-episode non-stationarity? (5) How gracefully does performance degrade as offset magnitude α is scaled from 0 (no offset) \rightarrow 1 (our evaluation setup)? (6) Can FORL serve as a plug-and-play module for different offline RL algorithms without retraining? Extended results, forecasts for the remaining series, and implementation details are provided in the Appendix. Results average 5 seeds, unless noted.

Baselines We compare our approach with the following baselines: DQL [14], Flow Q-learning (FQL) [23] are diffusion-based and flow-based offline RL policies, respectively, that do not incorporate forecast information. DQL+LAG- \bar{s} , FQL+LAG- \bar{s} extend DQL and FQL by using the sample mean of the forecasted states $\{\hat{s}_t\}_l$ at each timestep (using the constant per-episode predicted b^j). DQL+LAG- \tilde{s} similarly extends DQL using the median. DMBP+LAG is a variant of the Diffusion Model-Based Predictor (DMBP)[3] (a robust offline RL algorithm designed to mitigate state-observation perturbations at test time, detailed in Appendix D) that integrates forecasted states from *Zero-Shot FM* [10] into its state prediction module. By using the model learned from the offline data, DMBP+LAG aims to refine the forecasted states to make robust state estimations. The underlying policies throughout our experiments are identical policy checkpoints for both our method and the baselines.

Illustrative Example Figs. 6 and 16 illustrate an agent navigating the maze2d-large environment where the true position is labeled as “state”. The agent receives an observation indicating where the agent *believes* it is located due to unknown time-dependent factors. The candidate states predicted by the FORL diffusion model are shown as circles. Importantly, the agent’s $(\Delta o, a)$ -trajectory can reveal possible states for the agent. FORL’s diffusion model

Table 1: Normalized scores (mean \pm std.) for FORL framework and the baselines. Bold are the best values, and those not significantly different ($p > 0.05$, Welch’s t-test).

maze2d-medium	DQL	DQL+LAG- \bar{s}	DMBP+LAG	FORL (ours)
real-data-A	30.2 \pm 6.5	30.2 \pm 8.6	25.1 \pm 9.8	63.3 \pm 6.7
real-data-B	14.1 \pm 12.1	53.4 \pm 14.6	41.2 \pm 21.1	66.5 \pm 18.2
real-data-C	-2.3 \pm 3.3	56.7 \pm 18.5	56.9 \pm 18.4	86.3 \pm 15.7
real-data-D	4.7 \pm 5.0	36.9 \pm 16.3	38.5 \pm 14.2	103.4 \pm 11.9
real-data-E	3.5 \pm 8.8	8.7 \pm 6.0	11.4 \pm 2.8	51.2 \pm 13.7
Average	10.0	37.2	34.6	74.1
maze2d-large				
real-data-A	16.2 \pm 5.5	2.4 \pm 1.1	4.2 \pm 5.8	42.9 \pm 4.1
real-data-B	-0.5 \pm 2.9	5.5 \pm 9.0	15.0 \pm 14.6	34.9 \pm 9.2
real-data-C	0.9 \pm 1.7	16.6 \pm 7.5	26.8 \pm 8.4	45.6 \pm 4.1
real-data-D	3.0 \pm 6.6	8.6 \pm 3.2	13.4 \pm 4.1	58.4 \pm 6.5
real-data-E	-2.1 \pm 0.4	2.6 \pm 3.4	0.9 \pm 3.7	12.0 \pm 9.9
Average	3.5	7.1	12.1	38.8
antmaze-umaze-diverse				
real-data-A	22.7 \pm 3.0	41.0 \pm 5.2	45.7 \pm 4.8	65.3 \pm 8.7
real-data-B	24.2 \pm 3.5	48.3 \pm 7.0	62.5 \pm 13.2	74.2 \pm 10.8
real-data-C	21.7 \pm 3.5	50.4 \pm 8.3	60.4 \pm 3.9	78.8 \pm 8.5
real-data-D	5.8 \pm 2.3	26.7 \pm 6.3	29.2 \pm 5.9	75.8 \pm 8.0
real-data-E	6.0 \pm 6.8	58.0 \pm 16.6	59.3 \pm 7.6	81.3 \pm 6.9
Average	16.1	44.9	51.4	75.1
antmaze-medium-diverse				
real-data-A	31.0 \pm 6.5	40.0 \pm 5.7	39.7 \pm 4.0	44.0 \pm 7.9
real-data-B	23.3 \pm 4.8	48.3 \pm 4.8	43.3 \pm 16.0	55.8 \pm 7.0
real-data-C	10.0 \pm 2.3	48.3 \pm 3.4	49.6 \pm 3.7	52.9 \pm 9.5
real-data-D	11.7 \pm 5.4	46.7 \pm 7.5	41.7 \pm 6.6	64.2 \pm 8.6
real-data-E	18.7 \pm 4.5	27.3 \pm 8.6	26.0 \pm 5.5	26.7 \pm 4.7
Average	18.9	42.1	40.1	48.7
antmaze-large-diverse				
real-data-A	11.0 \pm 1.9	11.3 \pm 4.9	9.0 \pm 4.5	34.3 \pm 5.7
real-data-B	5.8 \pm 4.8	9.2 \pm 4.6	8.3 \pm 2.9	46.7 \pm 11.9
real-data-C	5.4 \pm 2.4	22.1 \pm 5.6	17.9 \pm 3.8	33.8 \pm 6.8
real-data-D	2.5 \pm 2.3	14.2 \pm 3.7	14.2 \pm 6.3	46.7 \pm 12.6
real-data-E	5.3 \pm 3.8	3.3 \pm 2.4	3.3 \pm 0.0	11.3 \pm 7.3
Average	6.0	12.0	10.5	34.6
kitchen-complete				
real-data-A	16.6 \pm 1.4	7.2 \pm 1.9	8.7 \pm 1.3	12.0 \pm 3.9
real-data-B	12.9 \pm 4.1	32.7 \pm 6.5	20.0 \pm 3.1	33.1 \pm 5.6
real-data-C	13.4 \pm 1.7	23.9 \pm 6.6	20.5 \pm 3.3	23.9 \pm 6.0
real-data-D	7.5 \pm 2.5	24.0 \pm 9.2	28.1 \pm 8.1	27.1 \pm 10.1
real-data-E	18.5 \pm 6.0	2.8 \pm 2.1	6.2 \pm 1.7	10.3 \pm 3.0
Average	13.8	18.1	16.7	21.3
cube-single-play				
	FQL	FQL+LAG- \bar{s}	FORL-F (ours)	
real-data-A	0.0 \pm 0.0	0.0 \pm 0.0	23.7 \pm 3.6	
real-data-B	0.0 \pm 0.0	15.0 \pm 7.0	60.0 \pm 7.0	
real-data-C	0.4 \pm 0.9	10.0 \pm 1.7	42.1 \pm 5.6	
real-data-D	0.0 \pm 0.0	0.8 \pm 1.9	70.0 \pm 13.0	
real-data-E	0.0 \pm 0.0	0.0 \pm 0.0	32.7 \pm 9.5	
Average	0.1	5.2	45.7	
antmaze-large-navigate				
real-data-A	22.7 \pm 2.2	1.3 \pm 0.7	24.3 \pm 4.3	
real-data-B	21.7 \pm 5.4	29.2 \pm 8.8	40.0 \pm 7.6	
real-data-C	5.0 \pm 1.1	34.6 \pm 6.7	55.8 \pm 3.7	
real-data-D	0.8 \pm 1.9	37.5 \pm 5.1	75.8 \pm 5.4	
real-data-E	10.0 \pm 4.1	3.3 \pm 0.0	15.3 \pm 8.7	
Average	12.0	21.2	42.2	

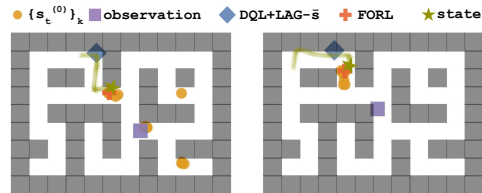


Figure 6: Visualization of states, predicted states as the agent navigates the environment.

(DM) component predicts these candidate states by using observation changes (Δo) and corresponding actions (a). The possible candidate regions where the agent can be are limited, and our model successfully captures these locations. FORL’s candidate selection module (DCM) uses the samples from the forecaster and the diffusion model to recover a close estimate for the state. In contrast, the baseline DQL+LAG- \bar{s} relies on the forecaster [10] for state predictions, which are significantly farther from the actual state. Consistent with the results in Fig. 7, FORL reduces prediction errors at test-time, thereby improving performance.

3.1 Results

FORL outperforms both pure forecasting (DQL+LAG- \bar{s}) and the two-stage strategy that first predicts offsets with a time-series model and then applies a noise-robust offline RL algorithm (DMBP+LAG). Its advantage is consistent across previously unseen non-stationary perturbations from five domains, each introducing a distinct univariate series into a separate state dimension at test time. We present the average normalized scores over the prediction length P across multiple episodes run in the D4RL [15] and OGBench [21] for each time-series in Table 1. We conduct pairwise Welch’s t-tests across all settings. Figure 7 plots the ℓ_2 norm between the ground-truth states s_t and those predicted by FORL and the baselines in the antmaze and maze2d environments. Consistent with the average scores, FORL achieves the lowest prediction error on average.

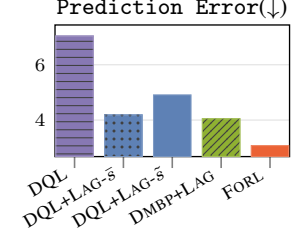


Figure 7: Prediction Error in recovering true agent state.

3.1.1 No Access to Past Offsets

We evaluate different variants of using DM and *Zero-Shot FM* when we do not have any access to past offsets in Fig. 8. **FORL-DM (DM)**: Diffusion Model utilizes the candidate states generated by the FORL’s diffusion model component (Section 2.2), which can be a multimodal distribution (Fig. 3). Compared to DM, the full FORL framework yields a 97.8% relative performance improvement. Notably, DM performs on par with our extended baselines that incorporate historical offsets and forecasting—DMBP+LAG, DQL+LAG- \bar{s} , and DQL+LAG- \bar{s} . Moreover, without access to historical offset information before evaluation, DM achieves a 151.4% improvement over DQL, demonstrating its efficacy as a standalone module trained solely on a standard, stationary offline RL dataset without offset labels. **H-LAG**: We maintain a history of offsets generated by DM over the most recent C episodes (excluding the evaluation interval P , since offsets are not revealed after episode termination at test-time). We then feed this history into the *Zero-Shot FM* to generate offset samples for the next P evaluation episodes. These samples are applied directly at test time. **H-LAG+DCM**: We initially follow the same procedure in H-LAG to obtain predictions from *Zero-Shot FM*. Then, we apply **DCM** to these predicted offsets and the candidate states generated by FORL’s diffusion model. We also compare against MED+DCM and MED+NOISE, simpler median-based heuristics detailed in Section G. Empirically, H-LAG+DCM outperforms H-LAG, demonstrating that DCM with FORL’s diffusion model can improve robustness. Overall, scores and prediction errors indicate that just using the samples from DM has better scores on average, while H-LAG+DCM is more stable in Fig. 15.

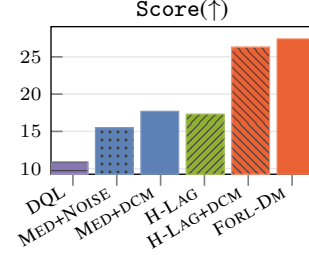


Figure 8: DM Ablations

3.1.2 Dimension-wise Closest Match (DCM) Ablations

We compare FORL (DCM) against four alternative fusion strategies. **FORL(KDE)**: For each dimension, we fit a kernel density estimator (KDE) on $\mathcal{D}_{\text{diffusion}} = \{s_t^{(0)}\}_k$ and then we evaluate that probability density function for each point in $\mathcal{D}_{\text{timeseries}}$. Then, we take the product of these densities in each dimension to obtain the weight for each sample \hat{s}_t^b . We obtain a single representative sample by taking the weighted average of samples in $\mathcal{D}_{\text{timeseries}}$. To ensure stability, when the sum of the weights is near zero, we use the mean of the $\mathcal{D}_{\text{timeseries}}$ as the states. We use Scott’s rule [24] to compute the bandwidth. **DM-FS- \bar{s}** , **DM-FS- \bar{s}** select the closest prediction from DM to the mean and median of the *Zero-Shot FM*’s predictions, respectively. **FORL (MAX)** constructs a diagonal multivariate distribution from the dimension-wise mean and standard deviation of the

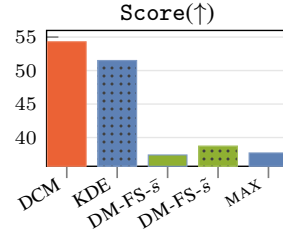


Figure 9: Candidate Selection

Table 2: **Normalized scores (mean \pm std.) for FORL and baselines on maze2d-large.** Bolds denote the best scores and those not significantly different (Welch’s t-test, $p > 0.05$). Suffixes -T and -R denote the use of TD3+BC [2] and RORL [25], respectively.

maze2d-large	Td3Bc Policy				RORL Policy			
	Td3Bc	Td3Bc+LAG- \bar{s}	DMBP+LAG-T	FORL (ours)-T	RORL	RORL+LAG- \bar{s}	DMBP+LAG-R	FORL (ours)-R
real-data-A	14.7 \pm 5.7	2.5 \pm 2.7	4.8 \pm 3.9	20.7 \pm 3.5	12.2 \pm 2.3	13.0 \pm 2.0	4.3 \pm 5.0	56.9 \pm 3.0
real-data-B	-0.9 \pm 2.0	4.6 \pm 8.9	11.7 \pm 12.6	56.8 \pm 14.4	1.2 \pm 5.5	13.1 \pm 14.7	28.5 \pm 11.7	98.5 \pm 19.0
real-data-C	0.8 \pm 1.9	21.6 \pm 8.4	29.5 \pm 13.7	56.9 \pm 14.6	3.1 \pm 0.9	60.6 \pm 8.5	39.4 \pm 6.1	139.0 \pm 15.1
real-data-D	2.5 \pm 4.4	14.9 \pm 4.3	14.4 \pm 6.8	29.5 \pm 10.3	-1.6 \pm 0.7	17.9 \pm 6.8	17.5 \pm 6.0	33.1 \pm 2.3
real-data-E	-2.3 \pm 0.2	1.0 \pm 4.2	2.0 \pm 3.9	8.0 \pm 4.2	-0.9 \pm 2.0	3.3 \pm 4.4	2.2 \pm 4.5	32.2 \pm 15.3
Average	3.0	8.9	12.5	34.4	2.8	21.6	18.4	71.9

forecasted states, then selects the sample predicted by our diffusion model with the highest likelihood under that distribution. Although all baselines fuse information using the same two sets generated by the diffusion model and *Zero-Shot FM*, DCM has higher performance. In Table 8 we compute the maximum, minimum, and mean prediction error values over the test episodes used in Fig. 6. FORL (DCM) yields significantly stable prediction errors (Maximum Error \downarrow :**2.40**) for both maximum error and mean error compared to FORL (MAX) (Maximum Error \downarrow :**9.33**) demonstrating its robustness.

3.1.3 Intra-episode Non-stationarity

Our framework can natively handle intra-episode offsets, where the offset changes every $f = 50$ timesteps. In this setting, the offsets become available after the episode terminates, but the agent is subject to a time-dependent unknown offset within the episode. Zero-shot forecasting foundation module can generate samples before the episode begins. Our diffusion model (FORL-DM) itself does not rely on the forecasts of the foundation module and only tracks observation changes and actions which are invariant to the offsets. The DCM can adaptively fuse information from both models at each timestep without requiring any hyperparameters. Table 10 and Fig. 10 show the average scores for DQL vs. FORL-DM and DQL+LAG- \bar{s} vs. FORL. Among the algorithms that do not use any past ground truth offsets DQL and FORL-DM, only using the diffusion model of FORL significantly increases performance. When we have access to past offsets, FORL obtains a superior performance. This shows that our method covers both cases, when information is available and not available, even when offsets are not constant throughout the episode.

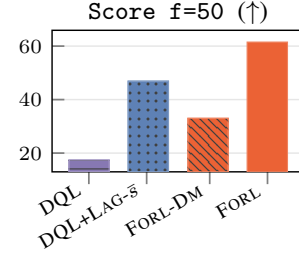


Figure 10: Intra-Episode Performance

3.1.4 Offset-Scaling

We scale the offsets with α across all maze experiments. We conduct experiments in 5 environments (all antmaze and maze2d used in Table 1) across 5 time-series dataset setups with $\alpha \in \{0, 0.25, 0.5, 0.75, 1.0\}$, where $\alpha = 0$ is the standard offline RL environment used during training and $\alpha = 1.0$ is our evaluation setup. The results show that FORL outperforms the baselines, confirming its robustness. Even a small scaling of 0.25 results in a sudden drop in performance, whereas FORL only experiences a gradual decrease in Figure 11. Detailed results for each environment and α pairs are provided in Appendix Figure 13.

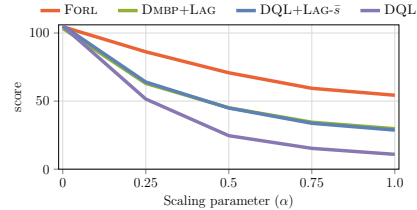


Figure 11: Impact of offset scaling (α) on average normalized scores.

3.1.5 Policy-Agnostic

In the maze2d-large experiments (in Table 2, maze2d-medium in Appendix Table 3), we use Robust Offline RL (RORL) [25], and TD3BC [2] offline RL algorithms instead of DQL [14], to analyze the effect of offline RL policy choice during evaluation. RORL+LAG- \bar{s} and TD3BC+LAG- \bar{s} extend RORL and TD3BC by using the sample mean of the forecasted states $\{\hat{s}_t\}_l$ at each timestep (using the constant per-episode predicted b^j). Results indicate that using a robust offline RL algorithm during training significantly increases performance (71.9) compared to DQL (38.8) and TD3BC (34.4) at test time when used with FORL, no increase when used alone, and a marginal increase with Lag-Llama and DMBP+LAG. We observe similar performance gains when applying FORL to other

policies (Section E), including Implicit Q-Learning (IQL) [26] and FQL [23], as detailed in Table 4 and Table 7.

4 Related Work

Reinforcement Learning in Non-Stationary Environments Existing works in non-stationary reinforcement learning (RL) predominantly focus on adapting to changing transition dynamics and reward functions. Ackermann et al. [27] propose an offline RL framework that incorporates structured non-stationarity in reward and transition functions by learning hidden task representations and predicting them at test time. Although our work also investigates the intersection of non-stationary environments and offline RL, we assume stationarity during training. To learn adaptive policies *online*, meta-learning algorithms have been proposed as a promising approach [28–30]. Al-Shedivat et al. [29] explores a competitive multi-agent environment where transition dynamics change. While these approaches provide valuable insights, they often require samples from the current environment and struggle in non-trivial non-stationarity, highlighting the need for more future-oriented methods [9, 31]. Examples of such future-oriented approaches include Proactively Synchronizing Tempo (ProST) [9] and Prognosticator [31], which address the evolution of transition and reward functions over time. ProST leverages a forecaster, namely, Auto-Regressive Integrated Moving Average (ARIMA), and a model predictor to optimize for future policies in environments to overcome the time-synchronization issue in time-elapsing MDPs. This approach aligns with our focus on time-varying environments and similarly utilizes real-world finance (e.g., stock price) time-series datasets to model non-stationarity. Both ProST and Prognosticator assume that states are fully observable during testing and that online interaction with the environment is possible during training—conditions that are not always feasible in the real world. Instead, our approach assumes that states are not fully observable and that direct interaction with the environment during training is not feasible, necessitating that the policy be learned exclusively from a pre-collected dataset.

Robust offline RL Testing-time robust offline RL methods DMBP [3], RORL [25] examine scenarios where a noise-free, stationary dataset is used for training, but corruption is introduced during testing. This is distinct from [3], training-time robust offline RL [32, 33], which assumes a corrupted training dataset. Both RORL [25] and DMBP [3] assume access only to a clean, uncorrupted offline RL dataset, as FORL, and they are evaluated in a perturbed environment. To the best of our knowledge, FORL is the first work to extend this setting to a non-Markovian, time-evolving, non-stationary deployment environment. We focus on time-dependent exogenous factors from real-data that are aligned with the definition of a non-stationary environment [6].

Diffusion models in offline RL Diffusion models [12] have seen widespread adoption in RL [34, 35] due to their remarkable expressiveness, particularly in representing multimodal distributions, scalability, and stable training properties. In the context of offline RL, diffusion models have been used for representing policies [14, 36–38], planners [39, 40], data synthesis [41, 42], and removing noise [3]. Notably, Diffusion Q-learning [14] leverages conditional diffusion model policies to learn from offline RL datasets, maintaining proximity to behavior policy while utilizing Q-value function guidance. In contrast, our method harnesses diffusion models to learn from a sequence of actions and effect tuples, leveraging the multimodal capabilities of diffusion models to identify diverse candidate locations of the hidden states.

5 Conclusion

We introduce **Forecasting in Non-stationary Offline RL (FORL)**, a novel framework designed to be robust to passive non-stationarities that arise at test time. This is crucial when an agent trained on an offline RL dataset is deployed in a non-stationary environment or when the environment begins to exhibit partial observability due to unknown, time-varying factors. FORL leverages diffusion probabilistic models and zero-shot time series foundation models to correct unknown offsets in observations, thereby enhancing the adaptability of learned policies. Our empirical results across diverse time-series datasets, OGBench [21] and D4RL [15] benchmarks demonstrate that FORL not only bridges the gap between time-series forecasting and non-stationary offline RL but also consistently outperforms the baselines. Our approach is currently limited by assuming additive perturbations. For future work, we plan to extend our work to more general observation transformations.

Acknowledgments and Disclosure of Funding

Georg Martius is a member of the Machine Learning Cluster of Excellence, EXC number 2064/1 – Project number 390727645. Co-funded by the European Union (ERC, REAL-RL, 101045454). Views and opinions expressed are, however, those of the author(s) only and do not necessarily reflect those of the European Union or the European Research Council. Neither the European Union nor the granting authority can be held responsible for them. This work was supported by the German Federal Ministry of Education and Research (BMBF): Tübingen AI Center, FKZ: 01IS18039A. This work was in part supported by INVERSE project (101136067) funded by the European Union and JSPS KAKENHI Grant Numbers JP23K24926, JP25H01236. The numerical calculations reported in this paper were partially performed at TUBITAK ULAKBIM, High Performance and Grid Computing Center (TRUBA resources). The authors would like to thank Tomáš Daniš, René Geist, Ji Shi, and Leonard Franz for their valuable comments on the manuscript.

References

- [1] Sergey Levine, Aviral Kumar, George Tucker, and Justin Fu. Offline reinforcement learning: Tutorial, review, and perspectives on open problems. *CoRR*, abs/2005.01643, 2020. URL <https://arxiv.org/abs/2005.01643>.
- [2] Scott Fujimoto and Shixiang Gu. A minimalist approach to offline reinforcement learning. In A. Beygelzimer, Y. Dauphin, P. Liang, and J. Wortman Vaughan, editors, *Advances in Neural Information Processing Systems*, 2021.
- [3] YANG Zhihe and Yunjian Xu. Dmbp: Diffusion model-based predictor for robust offline reinforcement learning against state observation perturbations. In *The Twelfth International Conference on Learning Representations*, 2024.
- [4] Brandon Trabucco, Mariano Phielipp, and Glen Berseth. Anymorph: Learning transferable policies by inferring agent morphology. In *International Conference on Machine Learning*, pages 21677–21691. PMLR, 2022.
- [5] Amy Zhang, Clare Lyle, Shagun Sodhani, Angelos Filos, Marta Kwiatkowska, Joelle Pineau, Yarín Gal, and Doina Precup. Invariant causal prediction for block mdp. In *International Conference on Machine Learning*, pages 11214–11224. PMLR, 2020.
- [6] Khimya Khetarpal, Matthew Riemer, Irina Rish, and Doina Precup. Towards continual reinforcement learning: A review and perspectives. *Journal of Artificial Intelligence Research*, 75: 1401–1476, 2022.
- [7] Yash Chandak. *Reinforcement Learning for Non-stationary problems*. PhD thesis, PhD thesis, University of Massachusetts Amherst, 2022.
- [8] Annie Xie, James Harrison, and Chelsea Finn. Deep reinforcement learning amidst continual structured non-stationarity. In *International Conference on Machine Learning*, pages 11393–11403. PMLR, 2021.
- [9] Hyunin Lee, Yuhao Ding, Jongmin Lee, Ming Jin, Javad Lavaei, and Somayeh Sojoudi. Tempo adaptation in non-stationary reinforcement learning. In *Thirty-seventh Conference on Neural Information Processing Systems*, 2023.
- [10] Kashif Rasul, Arjun Ashok, Andrew Robert Williams, Hena Ghonia, Rishika Bhagwatkar, Arian Khorasani, Mohammad Javad Darvishi Bayazi, George Adamopoulos, Roland Riachi, Nadhir Hassen, Marin Biloš, Sahil Garg, Anderson Schneider, Nicolas Chapados, Alexandre Drouin, Valentina Zantedeschi, Yuriy Nevmyvaka, and Irina Rish. Lag-llama: Towards foundation models for time series forecasting. *arXiv preprint arXiv:2310.08278*, 2023.
- [11] Jonathan Ho, Ajay Jain, and Pieter Abbeel. Denoising diffusion probabilistic models. In H. Larochelle, M. Ranzato, R. Hadsell, M.F. Balcan, and H. Lin, editors, *Advances in Neural Information Processing Systems*, volume 33, pages 6840–6851. Curran Associates, Inc., 2020.

- [12] Jascha Sohl-Dickstein, Eric A. Weiss, Niru Maheswaranathan, and Surya Ganguli. Deep unsupervised learning using nonequilibrium thermodynamics. *CoRR*, abs/1503.03585, 2015. URL <https://arxiv.org/abs/1503.03585>.
- [13] Calvin Luo. Understanding diffusion models: A unified perspective. *arXiv preprint arXiv:2208.11970*, 2022. URL <https://arxiv.org/abs/2208.11970>.
- [14] Zhendong Wang, Jonathan J Hunt, and Mingyuan Zhou. Diffusion policies as an expressive policy class for offline reinforcement learning. In *The Eleventh International Conference on Learning Representations*, 2023.
- [15] Justin Fu, Aviral Kumar, Ofir Nachum, George Tucker, and Sergey Levine. D4rl: Datasets for deep data-driven reinforcement learning. *arXiv preprint arXiv:2004.07219*, 2020. URL <https://arxiv.org/abs/2004.07219>.
- [16] Leslie Pack Kaelbling, Michael L Littman, and Anthony R Cassandra. Planning and acting in partially observable stochastic domains. *Artificial intelligence*, 101(1-2):99–134, 1998.
- [17] Blai Bonet. Deterministic pomdps revisited. *arXiv preprint arXiv:1205.2659*, 2012. URL <https://arxiv.org/abs/1205.2659>.
- [18] Yang Song, Jascha Sohl-Dickstein, Diederik P Kingma, Abhishek Kumar, Stefano Ermon, and Ben Poole. Score-based generative modeling through stochastic differential equations. *arXiv preprint arXiv:2011.13456*, 2020.
- [19] Zhisheng Xiao, Karsten Kreis, and Arash Vahdat. Tackling the generative learning trilemma with denoising diffusion gans. *arXiv preprint arXiv:2112.07804*, 2021.
- [20] Calvin Luo. Understanding diffusion models: A unified perspective, 2022. URL <https://arxiv.org/abs/2208.11970>.
- [21] Seohong Park, Kevin Frans, Benjamin Eysenbach, and Sergey Levine. Ogbench: Benchmarking offline goal-conditioned rl. In *International Conference on Learning Representations (ICLR)*, 2025.
- [22] Alexander Alexandrov, Konstantinos Benidis, Michael Bohlke-Schneider, Valentin Flunkert, Jan Gasthaus, Tim Januschowski, Danielle C. Maddix, Syama Rangapuram, David Salinas, Jasper Schulz, Lorenzo Stella, Ali Caner Türkmen, and Yuyang Wang. GluonTS: Probabilistic and Neural Time Series Modeling in Python. *Journal of Machine Learning Research*, 21(116): 1–6, 2020.
- [23] Seohong Park, Qiyang Li, and Sergey Levine. Flow q-learning. In *International Conference on Machine Learning (ICML)*, 2025.
- [24] David W Scot. Multivariate density estimation, 1992.
- [25] Rui Yang, Chenjia Bai, Xiaoteng Ma, Zhaoran Wang, Chongjie Zhang, and Lei Han. Rorl: Robust offline reinforcement learning via conservative smoothing. *Advances in neural information processing systems*, 35:23851–23866, 2022.
- [26] Ilya Kostrikov, Ashvin Nair, and Sergey Levine. Offline reinforcement learning with implicit q-learning. *CoRR*, abs/2110.06169, 2021. URL <https://arxiv.org/abs/2110.06169>.
- [27] Johannes Ackermann, Takayuki Osa, and Masashi Sugiyama. Offline reinforcement learning from datasets with structured non-stationarity. In *Reinforcement Learning Conference*, 2024.
- [28] Chelsea Finn, Aravind Rajeswaran, Sham Kakade, and Sergey Levine. Online meta-learning. In *International conference on machine learning*, pages 1920–1930. PMLR, 2019.
- [29] Maruan Al-Shedivat, Trapit Bansal, Yura Burda, Ilya Sutskever, Igor Mordatch, and Pieter Abbeel. Continuous adaptation via meta-learning in nonstationary and competitive environments. In *International Conference on Learning Representations*, 2018.

- [30] Suzan Ece Ada and Emre Ugur. Unsupervised meta-testing with conditional neural processes for hybrid meta-reinforcement learning. *IEEE Robotics and Automation Letters*, 9(10):8427–8434, 2024. doi: 10.1109/LRA.2024.3443496.
- [31] Yash Chandak, Georgios Theodorou, Shiv Shankar, Martha White, Sridhar Mahadevan, and Philip Thomas. Optimizing for the future in non-stationary mdps. In *International Conference on Machine Learning*, pages 1414–1425. PMLR, 2020.
- [32] Chenlu Ye, Rui Yang, Quanquan Gu, and Tong Zhang. Corruption-robust offline reinforcement learning with general function approximation. *Advances in Neural Information Processing Systems*, 36:36208–36221, 2023.
- [33] Xuezhou Zhang, Yiding Chen, Xiaojin Zhu, and Wen Sun. Corruption-robust offline reinforcement learning. In *International Conference on Artificial Intelligence and Statistics*, pages 5757–5773. PMLR, 2022.
- [34] Zhengbang Zhu, Hanye Zhao, Haoran He, Yichao Zhong, Shenyu Zhang, Yong Yu, and Weinan Zhang. Diffusion models for reinforcement learning: A survey. *arXiv preprint arXiv:2311.01223*, 2023.
- [35] Jiayu Chen, Bhargav Ganguly, Yang Xu, Yongsheng Mei, Tian Lan, and Vaneet Aggarwal. Deep generative models for offline policy learning: Tutorial, survey, and perspectives on future directions. *arXiv preprint arXiv:2402.13777*, 2024.
- [36] Longxiang He, Linrui Zhang, Junbo Tan, and Xueqian Wang. Diffcps: Diffusion model based constrained policy search for offline reinforcement learning. *arXiv preprint arXiv:2310.05333*, 2023.
- [37] Philippe Hansen-Estruch, Ilya Kostrikov, Michael Janner, Jakub Grudzien Kuba, and Sergey Levine. Idql: Implicit q-learning as an actor-critic method with diffusion policies. *arXiv preprint arXiv:2304.10573*, 2023. URL <https://arxiv.org/abs/2304.10573>.
- [38] Suzan Ece Ada, Erhan Oztop, and Emre Ugur. Diffusion policies for out-of-distribution generalization in offline reinforcement learning. *IEEE Robotics and Automation Letters*, 9(4): 3116–3123, 2024. doi: 10.1109/LRA.2024.3363530.
- [39] Michael Janner, Yilun Du, Joshua Tenenbaum, and Sergey Levine. Planning with diffusion for flexible behavior synthesis. In *International Conference on Machine Learning*, 2022.
- [40] Matthew Coleman, Olga Russakovsky, Christine Allen-Blanchette, and Ye Zhu. Discrete diffusion reward guidance methods for offline reinforcement learning. In *ICML 2023 Workshop: Sampling and Optimization in Discrete Space*, 2023.
- [41] Haoran He, Chenjia Bai, Kang Xu, Zhuoran Yang, Weinan Zhang, Dong Wang, Bin Zhao, and Xuelong Li. Diffusion model is an effective planner and data synthesizer for multi-task reinforcement learning. In A. Oh, T. Naumann, A. Globerson, K. Saenko, M. Hardt, and S. Levine, editors, *Advances in Neural Information Processing Systems*, volume 36, pages 64896–64917. Curran Associates, Inc., 2023.
- [42] Zhixuan Liang, Yao Mu, Mingyu Ding, Fei Ni, Masayoshi Tomizuka, and Ping Luo. Adaptdif-fuser: Diffusion models as adaptive self-evolving planners. *arXiv preprint arXiv:2302.01877*, 2023. URL <https://arxiv.org/abs/2302.01877>.
- [43] Scott Fujimoto, David Meger, and Doina Precup. Off-policy deep reinforcement learning without exploration. In *International Conference on Machine Learning*, 2018.
- [44] Noah Siegel, Jost Tobias Springenberg, Felix Berkenkamp, Abbas Abdolmaleki, Michael Neunert, Thomas Lampe, Roland Hafner, Nicolas Heess, and Martin Riedmiller. Keep doing what worked: Behavior modelling priors for offline reinforcement learning. In *International Conference on Learning Representations*, 2020.
- [45] Yecheng Jason Ma, Dinesh Jayaraman, and Osbert Bastani. Conservative offline distributional reinforcement learning. In A. Beygelzimer, Y. Dauphin, P. Liang, and J. Wortman Vaughan, editors, *Advances in Neural Information Processing Systems*, 2021. URL <https://openreview.net/forum?id=Z2vksUFuVst>.

- [46] Natasha Jaques, Asma Ghandeharioun, Judy Hanwen Shen, Craig Ferguson, Agata Lapedriza, Noah Jones, Shixiang Gu, and Rosalind Picard. Way off-policy batch deep reinforcement learning of implicit human preferences in dialog. *arXiv preprint arXiv:1907.00456*, 2019. URL <https://arxiv.org/abs/1907.00456>.
- [47] Yifan Wu, George Tucker, and Ofir Nachum. Behavior regularized offline reinforcement learning. *arXiv preprint arXiv:1911.11361*, 2019. URL <https://arxiv.org/abs/1911.11361>.
- [48] Xue Bin Peng, Aviral Kumar, Grace Zhang, and Sergey Levine. Advantage-weighted regression: Simple and scalable off-policy reinforcement learning. *arXiv preprint arXiv:1910.00177*, 2019.
- [49] Ashvin Nair, Abhishek Gupta, Murtaza Dalal, and Sergey Levine. Awac: Accelerating online reinforcement learning with offline datasets. *arXiv preprint arXiv:2006.09359*, 2020.
- [50] Sebastian Nowozin, Botond Cseke, and Ryota Tomioka. f-gan: Training generative neural samplers using variational divergence minimization. *Advances in neural information processing systems*, 29, 2016.
- [51] Aviral Kumar, Justin Fu, Matthew Soh, George Tucker, and Sergey Levine. Stabilizing off-policy q-learning via bootstrapping error reduction. *Advances in neural information processing systems*, 32, 2019.
- [52] Tianhe Yu, Aviral Kumar, Rafael Rafailov, Aravind Rajeswaran, Sergey Levine, and Chelsea Finn. COMBO: conservative offline model-based policy optimization. *CoRR*, abs/2102.08363, 2021. URL <https://arxiv.org/abs/2102.08363>.
- [53] Seohong Park, Kevin Frans, Sergey Levine, and Aviral Kumar. Is value learning really the main bottleneck in offline rl? *arXiv preprint arXiv:2406.09329*, 2024. URL <https://arxiv.org/abs/2406.09329>.
- [54] Bogdan Mazouze, Ilya Kostrikov, Ofir Nachum, and Jonathan J Tompson. Improving zero-shot generalization in offline reinforcement learning using generalized similarity functions. In S. Koyejo, S. Mohamed, A. Agarwal, D. Belgrave, K. Cho, and A. Oh, editors, *Advances in Neural Information Processing Systems*, volume 35, pages 25088–25101. Curran Associates, Inc., 2022.
- [55] Martin L Puterman. *Markov decision processes: discrete stochastic dynamic programming*. John Wiley & Sons, 2014.
- [56] Zhihe Yang and Yunjian Xu. DMBP: Diffusion model-based predictor for robust offline reinforcement learning against state observation perturbations. <https://github.com/zhyang2226/DMBP/tree/main>, 2024.
- [57] Hado Van Hasselt, Arthur Guez, and David Silver. Deep reinforcement learning with double q-learning. In *Proceedings of the AAAI conference on artificial intelligence*, volume 30, 2016.
- [58] Timothy P. Lillicrap, Jonathan J. Hunt, Alexander Pritzel, Nicolas Heess, Tom Erez, Yuval Tassa, David Silver, and Daan Wierstra. Continuous control with deep reinforcement learning. In Yoshua Bengio and Yann LeCun, editors, *4th International Conference on Learning Representations, ICLR 2016, San Juan, Puerto Rico, May 2-4, 2016, Conference Track Proceedings*, 2016.
- [59] Scott Fujimoto, Herke Hoof, and David Meger. Addressing function approximation error in actor-critic methods. In *International conference on machine learning*, pages 1587–1596. PMLR, 2018.
- [60] Jan Peters and Stefan Schaal. Reinforcement learning by reward-weighted regression for operational space control. In *Proceedings of the 24th international conference on Machine learning*, pages 745–750, 2007.
- [61] Qing Wang, Jiechao Xiong, Lei Han, Han Liu, Tong Zhang, et al. Exponentially weighted imitation learning for batched historical data. *Advances in Neural Information Processing Systems*, 31, 2018.

- [62] Denis Tarasov, Alexander Nikulin, Dmitry Akimov, Vladislav Kurenkov, and Sergey Kolesnikov. CORL: Research-oriented deep offline reinforcement learning library. In *3rd Offline RL Workshop: Offline RL as a "Launchpad"*, 2022.
- [63] Garrett Thomas. Implicit q-learning (iq) in pytorch. <https://github.com/gwthomas/IQL-PyTorch>, 2021.
- [64] Xingchao Liu, Chengyue Gong, and Qiang Liu. Flow straight and fast: Learning to generate and transfer data with rectified flow. *arXiv preprint arXiv:2209.03003*, 2022.
- [65] Xingchao Liu, Xiwen Zhang, Jianzhu Ma, Jian Peng, et al. InstafLOW: One step is enough for high-quality diffusion-based text-to-image generation. In *The Twelfth International Conference on Learning Representations*, 2023.
- [66] Kevin Frans, Danijar Hafner, Sergey Levine, and Pieter Abbeel. One step diffusion via shortcut models. *arXiv preprint arXiv:2410.12557*, 2024.
- [67] Zihan Ding, Chi Jin, Difan Liu, Haitian Zheng, Krishna Kumar Singh, Qiang Zhang, Yan Kang, Zhe Lin, and Yuchen Liu. Dollar: Few-step video generation via distillation and latent reward optimization. *arXiv preprint arXiv:2412.15689*, 2024.
- [68] Jiachen Li, Weixi Feng, Wenhui Chen, and William Yang Wang. Reward guided latent consistency distillation. *arXiv preprint arXiv:2403.11027*, 2024.
- [69] P.J. Huber, J. Wiley, and W. InterScience. *Robust statistics*. Wiley New York, 1981.
- [70] Martin A. Fischler and Robert C. Bolles. Random sample consensus: a paradigm for model fitting with applications to image analysis and automated cartography. *Commun. ACM*, 24(6): 381–395, June 1981. ISSN 0001-0782.
- [71] B. P. Welford. Note on a method for calculating corrected sums of squares and products. *Technometrics*, 4:419–420, 1962.
- [72] Donald Ervin Knuth. *The art of computer programming*, volume 3. Pearson Education, 1997.
- [73] Rakshitha Wathsadini Godahewa, Christoph Bergmeir, Geoffrey I. Webb, Rob Hyndman, and Pablo Montero-Manso. Monash time series forecasting archive. In *Thirty-fifth Conference on Neural Information Processing Systems Datasets and Benchmarks Track (Round 2)*, 2021.
- [74] Dua Dheeru and Efi Karra Taniskidou. Uci machine learning repository. <http://archive.ics.uci.edu/ml>, 2017.
- [75] David Salinas, Michael Bohlke-Schneider, Laurent Callot, Roberto Medico, and Jan Gasthaus. High-dimensional multivariate forecasting with low-rank gaussian copula processes. *Advances in neural information processing systems*, 32, 2019.
- [76] Guokun Lai, Wei-Cheng Chang, Yiming Yang, and Hanxiao Liu. Modeling long-and short-term temporal patterns with deep neural networks. In *The 41st international ACM SIGIR conference on research & development in information retrieval*, pages 95–104, 2018.
- [77] A. Alexandrov, K. Benidis, M. Bohlke-Schneider, V. Flunkert, J. Gasthaus, T. Januschowski, D. C. Maddix, S. Rangapuram, D. Salinas, J. Schulz, L. Stella, A. C. Türkmen, and Y. Wang. GluonTS: Probabilistic Time Series Modeling in Python. *arXiv preprint arXiv:1906.05264*, 2019.
- [78] Olaf Ronneberger, Philipp Fischer, and Thomas Brox. U-net: Convolutional networks for biomedical image segmentation. In *Medical image computing and computer-assisted intervention—MICCAI 2015: 18th international conference, Munich, Germany, October 5-9, 2015, proceedings, part III 18*, pages 234–241. Springer, 2015.
- [79] Zhendong Wang. Diffusion policies for offline rl (code). <https://github.com/Zhendong-Wang/Diffusion-Policies-for-Offline-RL>, 2023.
- [80] Zhihe Yang. Dmbp: Diffusion model based predictor (code tree). <https://github.com/zhyang2226/DMBP/tree/main>, 2023.

- [81] Diederik P. Kingma and Jimmy Ba. Adam: A method for stochastic optimization. In Yoshua Bengio and Yann LeCun, editors, *ICLR (Poster)*, 2015. URL <http://dblp.uni-trier.de/db/conf/iclr/iclr2015.html#KingmaB14>.
- [82] Ilya Kostrikov. Implicit q-learning (official jax implementation). https://github.com/ikostrikov/implicit_q_learning, 2021.
- [83] Tinkoff AI. Corl: Clean offline reinforcement learning. <https://github.com/tinkoff-ai/CORL>, 2022.
- [84] Seohong Park. Fql: Flow q-learning — official implementation. <https://github.com/seohongpark/fql>, 2025.
- [85] Scott Fujimoto. Td3_bc. https://github.com/sfujim/TD3_BC, 2018.
- [86] Rui Yang. Rorl: Repository. <https://github.com/YangRui2015/RORL>, 2022.
- [87] Emanuel Todorov, Tom Erez, and Yuval Tassa. Mujoco: A physics engine for model-based control. In *Intelligent Robots and Systems (IROS), 2012 IEEE/RSJ International Conference on Intelligent Robots and Systems*, pages 5026–5033. IEEE, 2012.
- [88] Artur Trindade. ElectricityLoadDiagrams20112014. UCI Machine Learning Repository, 2015. DOI: <https://doi.org/10.24432/C58C86>.
- [89] John D Hunter. Matplotlib: A 2d graphics environment. *Computing in science & engineering*, 9(03):90–95, 2007.

A Related Work: Continued

Offline Reinforcement Learning A high-level overview of existing work in offline reinforcement learning (RL) identifies three predominant strategies: policy constraint methods [14, 43, 44], pessimistic value function methods which assign low values to OOD actions [45], and model-based offline RL methods. Policy constraint methods actively avoid querying OOD actions during training by leveraging probabilistic metrics which can be explicit [46, 47], implicit [48, 49] f -divergence [50], or integral probability metrics [51]. These metrics ensure that the learned policy π_θ remains close to the behavior policy π_β that generated the offline RL dataset [1]. Similarly, pessimistic value function approaches regularize the value function or the Q-function to avoid overestimations in OOD regions. Model-based offline RL methods [52], on the other hand, focus on learning the environment’s dynamics benefiting from the strengths of supervised learning approaches. However, in the same vein, these methods are susceptible to the distribution shift problem in Offline RL [1]. We detail the offline RL algorithms used in our experiments in Section E.

Park et al. [53] emphasize the challenges of generalizing policies to test-time states which are not in the support of the offline RL dataset. While prior works have investigated the issue of generalization [38, 54], in testing-time robust RL methods [3] this challenge is exacerbated through the introduction of noise into the states by an unknown adversary.

B Background

B.1 Reinforcement Learning

Markov Decision Processes (MDPs) are often used to formalize Reinforcement Learning (RL). MDP is defined by the tuple $\mathcal{M} \doteq (\mathcal{S}, \mathcal{A}, \mathcal{T}, \mathcal{R}, \rho_0, \gamma)$ where \mathcal{S} is the state space, \mathcal{A} is the action space, \mathcal{T} is the transition function (which may be deterministic or stochastic), $\mathcal{R} : \mathcal{S} \times \mathcal{A} \rightarrow \mathbb{R}$ is the reward function, ρ_0 is the initial state distribution and $\gamma \in [0, 1]$ is the discount factor [55]. In online and off-policy RL algorithms an agent can interact with the environment using a parameterized policy $\pi_\theta(\mathbf{a}|s)$, to maximize the expected return $\mathbb{E}_\pi [\sum_t \gamma^t r(s_t, \mathbf{a}_t)]$. In contrast, offline RL requires the agent to learn from a static dataset $\mathcal{D} = \{(s_k, \mathbf{a}_k, s'_k, r_k)\}_{k=1}^N$ generated by a generally unknown behavior policy $\pi_\beta(\mathbf{a}|s)$ [1].

B.2 Non-Stationary Environments

We next review tangential definitions and formalisms used for non-stationary environments.

Definition B.1 (Partially Observable Markov Decision Processes [6, 7, 16]). A Partially Observable Markov Decision Process (POMDP) is given by the tuple

$$\hat{\mathcal{M}} = (\mathcal{S}, \mathcal{A}, \mathcal{O}, \mathcal{T}, \mathcal{R}, \mathbf{x}, \rho_0, \gamma),$$

where \mathcal{O} is the observation space and \mathbf{x} is the observation function. This function can be deterministic ($\mathbf{x} : \mathcal{S} \rightarrow \mathcal{O}$) [6, 17] or stochastic ($\mathbf{x}(o | s)$) for $o \in \mathcal{O}, s \in \mathcal{S}$ [7].

To capture a broader range of non-stationary RL scenarios, Khetarpal et al. [6] present a *general non-stationary RL* formulation, which allows each component of the underlying MDP or POMDP to evolve over time. Concretely, this time-varying tuple is denoted as $(\mathcal{S}(t), \mathcal{A}(t), \mathcal{T}(t), \mathcal{R}(t), \mathbf{x}(t), \mathcal{O}(t))$ where each element is represented by a function $\varphi(i, t)$, indicating its variation with time t and input i [6]. *Scope*, denoted by a set κ , specifies which of these components vary.

Definition B.2 (Scope of Non-Stationarity [6]). Given the general non-stationary RL framework, the *scope of non-stationarity* is the subset

$$\kappa \subseteq \{\mathcal{S}, \mathcal{A}, \mathcal{R}, \mathcal{T}, \mathbf{x}, \mathcal{O}\},$$

indicating which components of the environment evolve over time.

Notably, Chandak [7] defines Non-Stationary Decision Process (NSDP) as a sequence of POMDPs, with non-stationarity confined to the subset $\kappa \subseteq \{\mathcal{R}, \mathcal{T}, \mathbf{x}\}$, where the initial state distribution $\rho_{0,j}$ varies between POMDPs. Existing research in non-stationary RL largely focus on the episodic evolution of transition dynamics and reward functions [27]. In contrast, the evolution of observation

functions remains underexplored, despite its potential for real-world applicability and thus demand further investigation [6]. Handling inaccurate state information, is crucial in non-stationary RL since an agent may encounter non-stationarity due to its own imperfect perception of the state while the underlying physics of the environment remains unchanged [6].

B.3 Diffusion Models

Diffusion models [12] aim to model the data distribution with $p_\theta(\mathbf{x}_0) := \int p_\theta(\mathbf{x}_{0:T}) d\mathbf{x}_{1:T}$ from samples \mathbf{x}_0 in the dataset. The joint distribution $p_\theta(\mathbf{x}_{0:T})$, is modeled as a Markov chain, where $\mathbf{x}_1, \dots, \mathbf{x}_T$ are the latent variables with the same dimensionality as the data samples. The joint distribution is given by

$$p_\theta(\mathbf{x}_{0:T}) := \mathcal{N}(\mathbf{x}_T; \mathbf{0}, \mathbf{I}) \prod_{t=1}^T p_\theta(\mathbf{x}_{t-1} | \mathbf{x}_t) \quad (6)$$

where $p_\theta(\mathbf{x}_{t-1} | \mathbf{x}_t) := \mathcal{N}(\mathbf{x}_{t-1}; \boldsymbol{\mu}_\theta(\mathbf{x}_t, t), \boldsymbol{\Sigma}_\theta(\mathbf{x}_t, t))$. The forward process $q(\mathbf{x}_{1:T} | \mathbf{x}_0) := \prod_{t=1}^T q(\mathbf{x}_t | \mathbf{x}_{t-1})$ involves adding a small amount of Gaussian noise to the data sample at each diffusion timestep to obtain the latent variables following a variance schedule $\{\beta_t = 1 - \alpha_t \in (0, 1)\}_{t=1}^T$. Here, the encoder transitions are $q(\mathbf{x}_t | \mathbf{x}_{t-1}) := \mathcal{N}(\mathbf{x}_t; \sqrt{\alpha_t} \mathbf{x}_{t-1}, (1 - \alpha_t) \mathbf{I})$ [11]. Assuming we have access to the true data sample during training, using recursion and reparametrization trick we can obtain samples \mathbf{x}_t at any timestep t in closed form with $q(\mathbf{x}_t | \mathbf{x}_0) = \mathcal{N}(\mathbf{x}_t; \sqrt{\bar{\alpha}_t} \mathbf{x}_0, (1 - \bar{\alpha}_t) \mathbf{I})$ where $\bar{\alpha}_t = \prod_{i=1}^t \alpha_i$ [11]. During training, the evidence lower bound is oftentimes maximized by a simplified surrogate objective [11]. After learning the parameters of the reverse process, we can sample \mathbf{x}_T from $\mathcal{N}(\mathbf{x}_T; \mathbf{0}, \mathbf{I})$ to start generating samples through an iterative denoising procedure.

C Details on FORL

C.1 Conditional Diffusion Model Details

Our aim is to learn the reverse diffusion process, by modeling $p_\theta(\mathbf{s}_t^{(n-1)} | \mathbf{s}_t^{(n)}, \boldsymbol{\tau}_{(t,w)})$ as a Gaussian distribution $\mathcal{N}(\mathbf{s}_t^{(n-1)}; \boldsymbol{\mu}_\theta(\mathbf{s}_t^{(n)}, \boldsymbol{\tau}_{(t,w)}, n), \boldsymbol{\Sigma}_\theta(\mathbf{s}_t^{(n)}, \boldsymbol{\tau}_{(t,w)}, n))$ where n is the diffusion timestep and t is the RL timestep. We approximate this mean $\boldsymbol{\mu}_\theta(\mathbf{s}_t^{(n)}, \boldsymbol{\tau}_{(t,w)}, n)$ using a conditional noise model $\boldsymbol{\epsilon}_\theta$ with

$$\frac{\mathbf{s}_t^{(n)}}{\sqrt{\alpha(n)}} - \frac{1 - \alpha(n)}{\sqrt{1 - \bar{\alpha}(n)} \sqrt{\alpha(n)}} \boldsymbol{\epsilon}_\theta(\mathbf{s}_t^{(n)}, \boldsymbol{\tau}_{(t,w)}, n)$$

and fix the covariance $\boldsymbol{\Sigma}_\theta(\mathbf{s}_t^{(n)}, \boldsymbol{\tau}_{(t,w)}, n)$ with $(1 - \alpha(n)) \mathbf{I}$ [11]. Selecting a large number of diffusion timesteps can significantly increase the computational complexity of our algorithm. Hence, we use variance preserving stochastic differential equations (SDE) [18] following the formulation in [19] $\alpha(n) = e^{-(\beta_{\min}(\frac{1}{N}) + (\beta_{\max} - \beta_{\min}) \frac{2n-1}{2N^2})}$ where $\beta_{\max} = 10$ and $\beta_{\min} = 0.1$. We use the noise prediction model [11] with reverse diffusion chain

$$\mathbf{s}_t^{(n-1)} | \mathbf{s}_t^{(n)} = \frac{\mathbf{s}_t^{(n)}}{\sqrt{\alpha(n)}} - \frac{1 - \alpha(n)}{\sqrt{\alpha(n)}(1 - \bar{\alpha}(n))} \boldsymbol{\epsilon}_\theta(\mathbf{s}_t^{(n)}, \boldsymbol{\tau}_{(t,w)}, n) + \sqrt{1 - \alpha(n)} \boldsymbol{\epsilon} \quad (7)$$

where $\boldsymbol{\epsilon} \sim \mathcal{N}(\mathbf{0}, \mathbf{I})$ for $n = N, \dots, 1$, and $\boldsymbol{\epsilon} = \mathbf{0}$ for $n = 1$ [11].

By using the conditional version of the simplified surrogate objective from [11] we minimize the FORL model loss $\mathcal{L}_p(\theta)$, with Eq. (4) in the main paper. We can train the noise prediction model by sampling $\mathbf{s}_t^{(n)}$ for any diffusion timestep in the forward diffusion process, utilizing reparametrization and recursion [11]. We use the true data sample \mathbf{s}_t from the offline RL dataset to obtain the noisy state $\mathbf{s}_t^{(n)} = \sqrt{\bar{\alpha}(n)} \mathbf{s}_t + \sqrt{1 - \bar{\alpha}(n)} \boldsymbol{\epsilon}$. Leveraging our model's capacity to learn multimodal distributions, we generate a set of k samples (predicted state candidates) $\{\mathbf{s}_t^{(0)}\}$ in parallel from the reverse diffusion chain using Eq. (5).

Algorithm 2 Training

Require: Offline RL dataset \mathcal{D} **Initialize:** ϵ_θ 1: **for** each iteration **do**2: $\{(\tau_{(t,w)}, s_t)\} \sim \mathcal{D}$ 3: $n \sim \mathcal{U}(\{1, 2, \dots, N\})$ 4: $\epsilon \sim \mathcal{N}(\mathbf{0}, \mathbf{I})$

5: Take gradient descent step on

$$\nabla_\theta \left\| \epsilon - \epsilon_\theta \left(\sqrt{\bar{\alpha}_{(n)}} s_t + \sqrt{1 - \bar{\alpha}_{(n)}} \epsilon, \tau_{(t,w)}, n \right) \right\|^2$$

6: **end for**7: **return** ϵ_θ

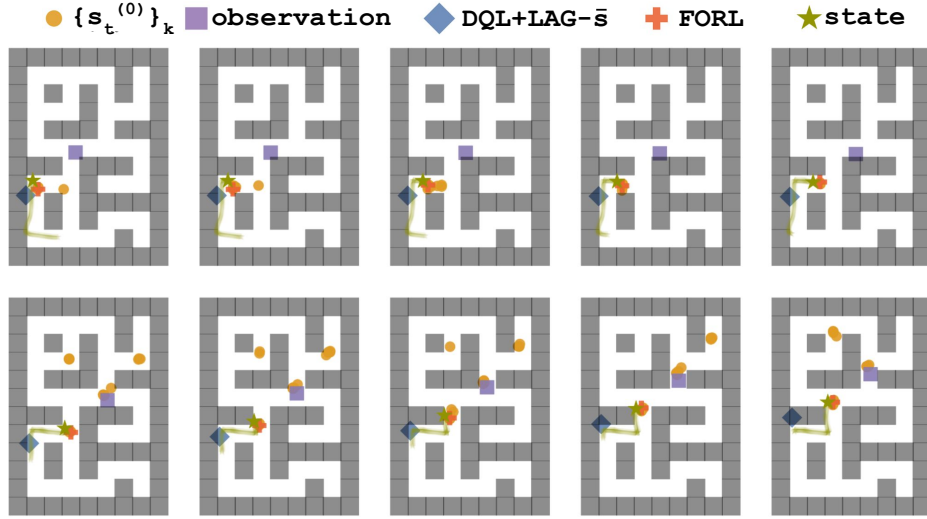


Figure 12: As the agent navigates in the maze2d-large environment [15], illustrations of states; predicted states from FORL (ours); FORL diffusion model predictions $\{s_t^{(0)}\}_k$; observations; and predicted states from DQL+LAG- \bar{s} are shown. Environment timesteps progress from left to right.

D Baselines

In this section we explain the baselines used in Table 1 and Figure 14. Diffusion Q-Learning (DQL) [14] serves as our base policy across all baselines and for our method in D4RL experiments [15]. Details on DQL are provided in Section E

D.1 DQL Extensions with Zero-Shot FM

For our baselines, we use a diffusion-based offline RL policy, DQL [14], with three variations:

- **DQL:** DQL policy directly generates actions conditioned on the observations. We include it to demonstrate how large episodic offsets degrade policy performance, and its consistently poor performance underscores the difficulty introduced by our offset settings.
- **DQL+LAG- \bar{s} :** We use *Zero-Shot FM* (Lag-Llama [10]) to forecast episodic offsets over a horizon of P episodes using pre-deployment offset history, and then subtract the mean predicted offset corresponding to that episode from the observations. Thus, DQL generates actions conditioned on the sample mean of the forecasted states $\{\hat{s}_t^b\}_l$. Although DQL+LAG- \bar{s} outperforms DQL, straightforward application of forecasting and decision making reveals performance degradation when offsets lack adaptive correction.

- **DQL+LAG- \bar{s}** : We use the sample median instead of the sample mean in DQL+LAG- \bar{s} , to mitigate outlier effects. As shown in Figure 14, median-based bias removal yields no significant improvement over the mean-based approach.

D.2 DMBP+LAG

We extend the Diffusion Model-Based Predictor (DMBP) [3], a model-based robust offline RL method trained on unperturbed D4RL benchmarks, to correct test-time state observation perturbations. DMBP has proven robust under Gaussian noise (varying σ), uniform noise, and adversarial perturbations—including maximum action-difference (MAD) and minimum Q-value (Min-Q) attacks. Similar to our framework, perturbed states are passed to DMBP, which removes the perturbations; the generated state is then fed to the policy. For a fair comparison, we adopt the policies also used in their work for our experiments, RORL [25] and TD3BC [2] alongside DQL.

DMBP+LAG extends DMBP with the forecasting module in our experiments. At each timestep, we remove offset biases using the sample mean of forecasted states $\{\hat{s}_t^b\}_l$ (as in DQL+LAG- \bar{s}) before DMBP correction. DMBP+LAG thus sequentially applies forecast-based offset compensation, followed by model based perturbation removal, and then queries the policy. DQL [14] remains the shared policy. A naive integration of DMBP relies on initial ground-truth states and underperforms.

For the evaluation of DMBP we use the open source code and the suggested hyperparameters available in [56]. To improve the performance of DMBP, we conducted evaluations at test-time and reported the best-performing results for a range of different diffusion timesteps. DMBP requires the diffusion timesteps to be manually defined based on different noise scales and types. Hence, we use the diffusion timesteps across a range of noise scales $\{0.15, 0.25, 0.5\}$ for maze and $\{0.05, 0.1, 0.15, 0.25\}$ for kitchen environments and identify that the best performance requires different noise scales across environment datasets. In particular, we report the best performing noise scale of 0.15 for the maze2d-medium environment, 0.25 for the maze2d-large environment, 0.5 for the antmaze-umaze-diverse environment, 0.15 for the antmaze-medium-diverse environment, 0.25 for the antmaze-large-diverse environment, 0.05 for kitchen-complete.

E Offline Reinforcement Algorithms

DQL [14] DQL [14] is an offline RL algorithm that uses policy regularization via a conditional diffusion model [11]. Wang et al. [14] shows that Gaussian policies lack the expressiveness needed to capture the possibly multimodal and skewed behavior policy in offline datasets, which, in turn, limits performance. To remedy this, DQL uses a conditional diffusion model for the behavior-cloning term, shown as the first part of Equation 8, based on a state-conditioned version of the simplified Denoising Diffusion Probabilistic Models (DDPM) objective [11]. To steer action generation toward high-reward regions, the policy improvement loss also includes Q-value guidance, shown as the second term below [14]

$$\mathbb{E}_{n \sim \mathcal{U}, (s, a) \sim \mathcal{D}, \epsilon \sim \mathcal{N}(0, I)} \left[\left\| \epsilon - \epsilon_\phi(\sqrt{\bar{\alpha}(n)} a + \sqrt{1 - \bar{\alpha}(n)} \epsilon, s, n) \right\|^2 \right] - \alpha \mathbb{E}_{s \sim \mathcal{D}, a^0 \sim \pi_\phi} [Q_\psi(s, a^0)]. \quad (8)$$

Here, a reverse diffusion process conditioned on state s , denoted by $\pi_\phi(a | s)$, represents the policy. The Q-networks are trained using the double Q-learning trick [57] and Bellman operator minimization [43, 58], with [14]

$$\mathbb{E}_{(s_t, a_t, s_{t+1}) \sim \mathcal{D}, a_{t+1}^0 \sim \pi_{\phi'}} \left[\left\| \left(r(s, a) + \gamma \min_{i=1,2} Q_{\psi'_i}(s_{t+1}, a_{t+1}^0) \right) - Q_{\psi_i}(s_t, a_t) \right\|^2 \right] \quad (9)$$

where a_{t+1}^0 is sampled from the diffusion policy conditioned on s_{t+1} , and $Q_{\psi_i}, Q_{\psi'_i}, \phi'$ denote the critic and target-critic networks, target policy network, respectively.

TD3BC [2] TD3BC [2] extends the Twin Delayed Deep Deterministic policy gradient algorithm (TD3) [59] to the offline RL setup. TD3BC incorporates a behavior cloning regularization term, normalizes state features within the offline RL dataset, and scales the Q-function using a hyperparameter

Table 3: **Normalized scores (mean \pm std.) for FORL and baselines with TD3BC and RORL on maze2d-medium.** Algorithms are grouped by their underlying policies—TD3 with Behavior Cloning (TD3+BC) [2] and Robust Offline Reinforcement Learning (RORL) [25] to highlight that performance variations stem from the algorithms themselves rather than the policies employed. Suffixes -T and -R denote the use of TD3+BC and RORL policies, respectively.

maze2d-medium	Td3Bc Policy				RORL Policy			
	Td3BC	Td3BC+LAG- \bar{s}	DMBP+LAG-T	FORL (ours)-T	RORL	RORL+LAG- \bar{s}	DMBP+LAG-R	FORL (ours)-R
real-data-A	37.4 \pm 9.5	16.2 \pm 5.1	16.2 \pm 7.3	22.1 \pm 6.6	80.7 \pm 14.2	57.9 \pm 8.6	47.8 \pm 10.2	52.7 \pm 5.0
real-data-B	3.6 \pm 2.3	6.1 \pm 4.4	14.4 \pm 8.1	28.6 \pm 19.0	37.8 \pm 7.5	85.9 \pm 19.8	91.0 \pm 21.6	109.6 \pm 19.5
real-data-C	-2.3 \pm 1.3	30.0 \pm 10.0	19.3 \pm 6.2	24.5 \pm 10.2	33.7 \pm 4.6	89.2 \pm 15.8	93.4 \pm 16.3	125.4 \pm 14.5
real-data-D	6.3 \pm 3.4	15.5 \pm 3.8	12.2 \pm 2.6	38.7 \pm 13.4	37.0 \pm 17.0	71.2 \pm 27.2	77.7 \pm 26.2	136.1 \pm 11.9
real-data-E	-3.7 \pm 1.5	9.7 \pm 5.2	11.5 \pm 6.6	15.1 \pm 8.8	60.9 \pm 13.5	10.0 \pm 7.3	14.2 \pm 8.6	61.2 \pm 14.6
Average	8.3	15.5	14.7	25.8	50.0	62.8	64.8	97.0

with an added normalization term. TD3BC is a straightforward yet effective method that is also computationally efficient. The results in Table 2 and Table 3 show that although extending TD3BC with the forecasting module (TD3BC+LAG- \bar{s}) and a combination of the forecasting module and a diffusion model-based predictor (DMBP+LAG-T) improves performance, FORL-T achieves better performance across a diverse range of non-stationarities.

RORL [25] RORL [25] addresses adversarial perturbations of the observation function by learning a conservative policy that aims to be robust to out-of-distribution (OOD) state and action pairs. To achieve this, it introduces a conservative smoothing mechanism that balances mitigating abrupt changes in the value function for proximate states and avoiding value overestimation in risky regions absent from the dataset. Concretely, RORL regularizes both the policy and the value function, leveraging bootstrapping Q-functions and conservative smoothing of the perturbed states. This formulation yields robust training under adversarial perturbations in the observation function while preserving strong performance even in unperturbed environments. However, although using RORL as our base policy improved performance in maze2d environments, FORL significantly outperforms both its naive usage, the extension with our forecasting module RORL+LAG- \bar{s} , and DMBP+LAG-R in Table 2 and Table 3. These results demonstrate that policies designed to be robust to sensor noise or adversarial attacks fail to cope with evolving observation functions that introduce non-stationarity into the environment.

IQL [26] Implicit Q-Learning [26] first learns a value function by expectile loss and a Q-function by Mean Squared Error (MSE) Loss without using the policy and instead using actions from the dataset. In doing so, they avoid approximating the values of unseen actions. Then, it learns the policy using advantage weighted regression [48, 49, 60, 61] using the learned Q-function and value function. We use the open-source implementation of IQL from [62] which references the source [63]. Results in Table 4 show FORL-I outperforms the baselines IQL, IQL+LAG- \bar{s} , and DMBP+LAG-I across all environments.

FQL [23] Flow Q-learning (FQL) [23] is a recent offline RL policy that shows strong performance on the OGBench [21]. We use FQL for the offline RL environments in OGBench and adopt the hyperparameters from the open-source implementation¹. Similar to DQL, which uses diffusion models, FQL can learn an expressive policy. FQL trains two policies: (i) a flow policy trained with flow matching on the offline RL dataset for behavior cloning conditioned on the state, and (ii) a one-step policy trained with a distillation loss using the flow policy [64–68] and a critic loss. This approach avoids expensive backpropagation through time; thus, it is fast during inference and training. Results in Tables 1 and 7 show FORL (also referred to as FORL (DCM)) outperforms the baselines when all baselines use FQL policy.

F Scaling Offsets

We conduct an analysis to quantify FORL’s sensitivity to different levels of non-stationarity. We scale the offset magnitude from 0 (standard D4RL offline RL environment [15] used in training) to 1 (our experiments) using scaling factors $\{0, 0.25, 0.5, 0.75, 1.0\}$, and report performance over

¹<https://github.com/seohongpark/fql/>

Table 4: **Normalized scores (mean \pm std.) for FORL and baselines with IQL.** Suffix -I denote the use of IQL algorithm [26].

maze2d-medium	IQL	IQL+LAG- \bar{s}	DMBP+LAG-I	FORL (ours)-I
real-data-A	39.5 \pm 7.8	16.0 \pm 4.9	12.2 \pm 7.7	19.5 \pm 2.9
real-data-B	3.7 \pm 7.3	13.1 \pm 8.7	14.0 \pm 9.5	32.3 \pm 13.1
real-data-C	-1.1 \pm 2.5	33.1 \pm 11.9	28.0 \pm 10.9	31.8 \pm 9.9
real-data-D	10.1 \pm 2.6	12.4 \pm 5.6	12.7 \pm 9.0	40.0 \pm 10.1
real-data-E	-4.5 \pm 0.2	12.4 \pm 5.2	9.9 \pm 2.9	24.0 \pm 8.4
Average	9.6	17.4	15.4	29.5
maze2d-large				
real-data-A	16.2 \pm 6.2	12.5 \pm 5.5	6.0 \pm 4.7	24.3 \pm 9.4
real-data-B	-0.6 \pm 2.6	3.3 \pm 7.7	13.5 \pm 10.5	42.8 \pm 9.8
real-data-C	0.1 \pm 1.5	27.8 \pm 13.1	27.9 \pm 5.5	46.7 \pm 9.2
real-data-D	1.2 \pm 3.7	11.2 \pm 7.4	8.0 \pm 7.5	23.9 \pm 8.4
real-data-E	-2.3 \pm 0.2	-1.5 \pm 1.1	1.5 \pm 4.1	7.9 \pm 7.2
Average	2.9	10.7	11.4	29.1
antmaze-umaze-diverse				
real-data-A	23.0 \pm 1.4	43.7 \pm 6.1	44.0 \pm 9.6	50.3 \pm 11.0
real-data-B	21.7 \pm 5.4	55.0 \pm 6.2	61.7 \pm 9.5	70.8 \pm 13.2
real-data-C	20.0 \pm 3.2	45.4 \pm 4.0	58.3 \pm 5.1	73.8 \pm 5.4
real-data-D	6.7 \pm 5.6	26.7 \pm 8.6	29.2 \pm 6.6	77.5 \pm 4.8
real-data-E	8.0 \pm 8.7	60.0 \pm 11.8	56.0 \pm 9.8	68.0 \pm 13.0
Average	15.9	46.1	49.8	68.1
antmaze-medium-diverse				
real-data-A	18.3 \pm 5.5	21.0 \pm 5.8	24.7 \pm 4.0	17.7 \pm 3.5
real-data-B	7.5 \pm 3.5	7.5 \pm 5.4	8.3 \pm 7.8	11.7 \pm 7.5
real-data-C	2.5 \pm 3.7	18.8 \pm 6.1	15.8 \pm 4.8	16.2 \pm 7.4
real-data-D	8.3 \pm 4.2	12.5 \pm 5.9	12.5 \pm 7.8	16.7 \pm 2.9
real-data-E	3.3 \pm 4.1	22.7 \pm 8.0	22.7 \pm 12.3	22.7 \pm 6.4
Average	8.0	16.5	16.8	17.0

five random seeds across five environments in maze2d and antmaze in Figure 13. This analysis delivers two key insights: first, FORL matches baseline performance on the stationary offline RL dataset on which it was trained; second, it maintains superior results throughout the full range of non-stationarity magnitudes. Crucially, FORL’s performance degrades gracefully as the magnitude of offsets increases, whereas DQL (without forecasting) suffers steep drops. Furthermore, both DMBP+LAG and DQL+LAG- \bar{s} decline in a similar manner. DMBP+LAG degrades slightly more gracefully than DQL+LAG- \bar{s} in maze2d-large and antmaze-umaze-diverse.

G What if we do not have access to past offsets?

To analyze the challenging identifiability issue arising from (i) non-smoothly varying offsets and (ii) the unobservability of ground truth offsets throughout the evaluation interval, we implement a set of methods for the setting where we never have delayed access to past ground truth offsets. Fig. 14 shows the average normalized scores and prediction accuracies over 25 environment–non-stationarity pairs across five random seeds in navigation control tasks with continuous state and action spaces. Overall, these methods underperform compared to FORL. Among the cases with no access to past offsets (see Fig. 15), the best-performing methods are our proposed candidate state generation module (FORL-DM) and H-LAG+DCM, a version of FORL that utilizes *Zero-Shot FM* in addition to DM which we detailed in Section 3.1.1.

FORL-DM (DM) FORL-DM, which we also refer to as DM for brevity, directly uses the state predicted by the diffusion model component. Given the multimodal nature of these candidate states,

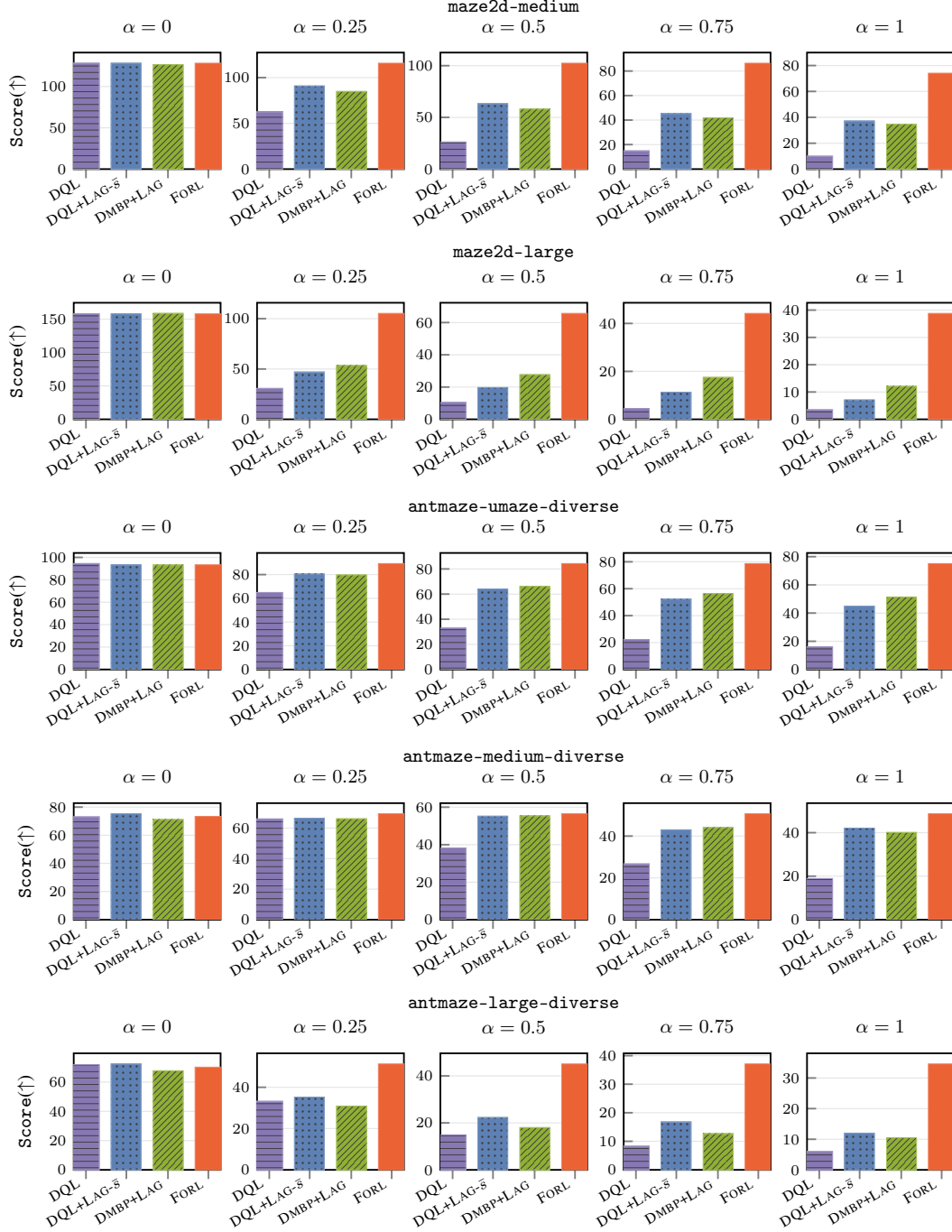


Figure 13: Average normalized scores of FORL (ours) and baselines across offset scaling factors $\alpha \in \{0, 0.25, 0.5, 0.75, 1\}$ in the maze2d-medium, maze2d-large, antmaze-umaze-diverse, antmaze-medium-diverse, antmaze-large-diverse environments. Scaling factor $\alpha = 0$ corresponds to a stationary D4RL [15] test environment; $\alpha = 1$ matches the original experimental configuration in Fig. 14. Results are averaged over 5 non-stationarities (real-data-A, real-data-B, real-data-C, real-data-D, real-data-E) and 5 random seeds.

this selection does not fully leverage our framework. Yet, DM outperforms the baselines when no past offsets are used. Additional comparisons in Table 6 with other standard statistical methods like

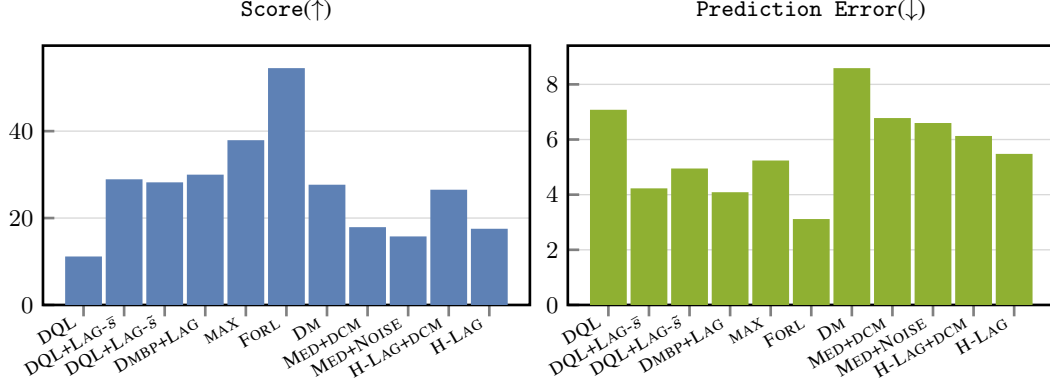


Figure 14: **Comparison of average normalized scores and prediction errors across all 25 experiments in D4RL[15]** between **FORL (ours)** and baseline methods, each evaluated over 5 random seeds. LAG denotes the integration of a zero-shot time-series foundation model [10]. While **FORL** and **MAX** also utilize this model, the subscripts are omitted for brevity.

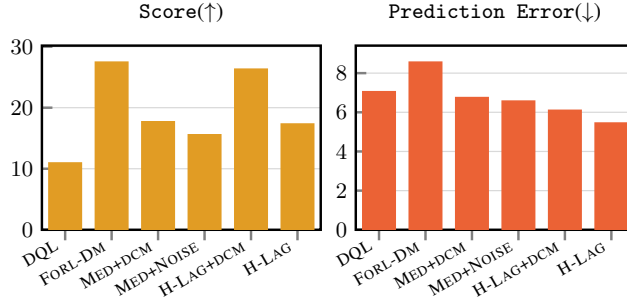


Figure 15: **Performance comparison without access to past offsets.** Average normalized scores and prediction errors for **FORL (ours)** versus baselines, aggregated over 25 experiments (5 random seeds each) in D4RL[15]. LAG denotes the integration of a zero-shot time-series foundation model [10]. However, in this setting *Zero-Shot FM* uses the samples from DM instead of past offsets.

DM-MAD, DM-RANSAC, DM-RUNNING- μ , DM-RUNNING- μ -p indicate that only using the sample predicted by the diffusion model yields higher scores on average.

MED+DCM We compute the median of the predicted offsets from the previous episode, beginning with the first episode predicted by FORL’s diffusion model. We then fit a Gaussian distribution centered at this median and sample l offsets from it, matching the sample count of *Zero-Shot FM*. Next, we apply **DCM** to these samples with the candidates generated by the diffusion model.

MED+NOISE We begin by computing the median offset produced by the diffusion model during the first evaluation episode similar to MED+DCM. Thereafter, we treat these offsets as evolving according to a random walk, where each offset is predicted as the previous value with white noise increments.

DM-MAD DM-MAD follows a state estimation based on robust statistics [69]. DM-MAD computes the coordinate-wise median of the differences between the observation and each denoiser prediction and discards any sample whose absolute deviation from this median exceeds $\epsilon \times$ Median Absolute Deviation (MAD). Then, it takes the median of the remaining inliers to obtain a robust offset estimate and subtracts that offset from the observation to obtain the state \hat{s}_t .

DM-RANSAC DM-RANSAC is a RANdom Sample Consensus (RANSAC) [70] based state estimation using the samples from our DM. DM-RANSAC calculates the offsets using the states generated by our DM and the observation, setting an adaptive per-dimension threshold as $\epsilon \times$ MAD.

Table 5: **Normalized scores (mean \pm std.) for no-access to past offsets setting.** This table shows the performance comparison of other heuristics variants using FORL-DM or leveraging a *Zero-Shot FM* in combination with FORL-DM when we do not have access to past offsets.

maze2d-medium	DQL	MED+NOISE	MED+DCM	H-LAG	H-LAG+DCM	FORL-DM
real-data-A	30.2 \pm 6.5	27.4 \pm 14.5	27.4 \pm 12.2	29.7 \pm 11.3	48.8 \pm 10.0	55.2 \pm 10.6
real-data-B	14.1 \pm 12.1	23.9 \pm 14.3	33.1 \pm 19.5	4.5 \pm 12.3	50.3 \pm 12.9	56.8 \pm 24.7
real-data-C	-2.3 \pm 3.3	17.6 \pm 8.1	-2.6 \pm 2.5	26.5 \pm 5.4	30.3 \pm 5.6	52.8 \pm 10.3
real-data-D	4.7 \pm 5.0	18.9 \pm 9.1	64.1 \pm 12.7	18.2 \pm 13.7	1.8 \pm 3.8	60.1 \pm 20.2
real-data-E	3.5 \pm 8.8	21.8 \pm 15.6	-2.1 \pm 1.6	56.7 \pm 11.6	45.7 \pm 12.4	60.5 \pm 18.2
Average	10.0	21.9	24.0	27.1	35.4	57.1
maze2d-large						
real-data-A	16.2 \pm 5.5	6.4 \pm 2.9	-1.8 \pm 0.5	7.1 \pm 3.9	7.3 \pm 2.0	11.1 \pm 4.3
real-data-B	-0.5 \pm 2.9	-0.1 \pm 1.7	-1.4 \pm 1.7	-1.4 \pm 2.3	0.9 \pm 4.5	13.4 \pm 10.3
real-data-C	0.9 \pm 1.7	3.2 \pm 4.7	-2.0 \pm 0.6	3.4 \pm 2.0	0.5 \pm 1.7	9.4 \pm 2.5
real-data-D	3.0 \pm 6.6	3.7 \pm 6.8	47.6 \pm 16.4	1.0 \pm 4.5	2.9 \pm 4.0	7.4 \pm 7.2
real-data-E	-2.1 \pm 0.4	3.8 \pm 4.7	-0.5 \pm 3.7	1.8 \pm 2.7	7.2 \pm 2.3	7.7 \pm 7.6
Average	3.5	3.4	8.4	2.4	3.8	9.8
antmaze-umaze-diverse						
real-data-A	22.7 \pm 3.0	8.3 \pm 2.4	8.3 \pm 4.7	32.3 \pm 6.3	62.7 \pm 11.2	48.7 \pm 9.1
real-data-B	24.2 \pm 3.5	9.2 \pm 5.4	25.0 \pm 13.2	41.7 \pm 5.1	33.3 \pm 2.9	56.7 \pm 8.1
real-data-C	21.7 \pm 3.5	10.8 \pm 7.7	75.8 \pm 6.4	36.7 \pm 3.2	59.2 \pm 11.5	55.0 \pm 8.7
real-data-D	5.8 \pm 2.3	17.5 \pm 11.6	6.7 \pm 6.3	10.8 \pm 2.3	42.5 \pm 7.5	54.2 \pm 7.2
real-data-E	6.0 \pm 6.8	50.0 \pm 13.5	2.0 \pm 3.0	14.0 \pm 8.3	42.7 \pm 11.9	53.3 \pm 7.8
Average	16.1	19.2	23.6	27.1	48.1	53.6
antmaze-medium-diverse						
real-data-A	31.0 \pm 6.5	34.3 \pm 10.4	55.0 \pm 6.8	15.0 \pm 4.9	17.3 \pm 6.3	4.3 \pm 0.9
real-data-B	23.3 \pm 4.8	15.8 \pm 9.9	42.5 \pm 4.6	33.3 \pm 4.2	28.3 \pm 3.5	6.7 \pm 4.8
real-data-C	10.0 \pm 2.3	23.3 \pm 5.4	10.0 \pm 4.3	31.2 \pm 4.9	40.4 \pm 6.7	4.6 \pm 1.7
real-data-D	11.7 \pm 5.4	26.7 \pm 6.3	33.3 \pm 15.9	9.2 \pm 3.5	36.7 \pm 6.8	3.3 \pm 3.5
real-data-E	18.7 \pm 4.5	26.7 \pm 18.1	0.0 \pm 0.0	14.7 \pm 5.6	46.0 \pm 16.2	6.0 \pm 4.3
Average	18.9	25.4	28.2	20.7	33.7	5.0
antmaze-large-diverse						
real-data-A	11.0 \pm 1.9	5.0 \pm 3.9	1.3 \pm 1.4	9.0 \pm 1.9	11.3 \pm 4.1	11.0 \pm 3.0
real-data-B	5.8 \pm 4.8	7.5 \pm 3.5	5.0 \pm 5.4	9.2 \pm 1.9	7.5 \pm 1.9	11.7 \pm 4.6
real-data-C	5.4 \pm 2.4	5.4 \pm 2.4	1.7 \pm 0.9	10.8 \pm 2.7	12.9 \pm 5.8	12.1 \pm 2.7
real-data-D	2.5 \pm 2.3	15.8 \pm 6.2	11.7 \pm 4.6	8.3 \pm 6.6	14.2 \pm 6.3	15.0 \pm 9.6
real-data-E	5.3 \pm 3.8	5.3 \pm 3.0	1.3 \pm 1.8	8.7 \pm 3.0	6.0 \pm 2.8	8.7 \pm 5.1
Average	6.0	7.8	4.2	9.2	10.4	11.7

Then, it repeatedly samples a random offset candidate and chooses the candidate whose inlier set (differences within that threshold) is the largest. Then, it takes the average of those inliers to estimate the offset.

DM-RUNNING- μ DM-RUNNING- μ computes a numerically stable, global running mean [71, 72] of offsets from DM aggregated across all timesteps and episodes.

DM-RUNNING- μ -p DM-RUNNING- μ -p computes an online average of offsets [71, 72] from DM (Running- μ) per episode p . Unlike DM-RUNNING- μ , in DM-RUNNING- μ -p the statistics are reset to zero at the beginning of each episode.

H Candidate Selection

The results in Table 9, Table 8, and Table 7 show that FORL (DCM) more consistently performs better than other methods. Although the KDE-based FORL(KDE) method performs well

Table 6: **Additional results for no-access to past offsets setting.** We present alternative ways of using FORL’s diffusion model (DM) component when we do not have access to past offsets.

maze2d-medium	DM-MAD	DM-RANSAC	DM-RUNNING- μ	DM-RUNNING- μ -p	FORL-DM
real-data-A	44.3 \pm 10.6	46.8 \pm 12.4	37.8 \pm 13.6	37.4 \pm 8.7	55.2 \pm 10.6
real-data-B	46.8 \pm 19.0	44.6 \pm 17.1	42.4 \pm 24.5	51.6 \pm 11.7	56.8 \pm 24.7
real-data-C	46.4 \pm 10.9	44.5 \pm 10.1	41.8 \pm 16.0	61.7 \pm 14.1	52.8 \pm 10.3
real-data-D	47.7 \pm 22.9	49.9 \pm 23.2	44.4 \pm 24.1	52.5 \pm 13.3	60.1 \pm 20.2
real-data-E	42.9 \pm 10.6	52.4 \pm 15.7	48.3 \pm 18.8	24.2 \pm 12.2	60.5 \pm 18.2
Average	45.6	47.6	42.9	45.5	57.1

Table 7: **Normalized scores (mean \pm std.) for FORL framework and the baselines.**

cube-single-play	FQL	FORL-DM-F	FQL+LAG- \bar{s}	FORL (MAX)-F	FORL(KDE)-F	FORL-F (ours)
real-data-A	0.0 \pm 0.0	3.0 \pm 1.4	0.0 \pm 0.0	0.0 \pm 0.0	0.0 \pm 0.0	23.7 \pm 3.6
real-data-B	0.0 \pm 0.0	6.7 \pm 5.6	15.0 \pm 7.0	43.3 \pm 4.8	2.5 \pm 2.3	60.0 \pm 7.0
real-data-C	0.4 \pm 0.9	4.6 \pm 1.7	10.0 \pm 1.7	39.6 \pm 4.4	38.3 \pm 3.8	42.1 \pm 5.6
real-data-D	0.0 \pm 0.0	2.5 \pm 2.3	0.8 \pm 1.9	7.5 \pm 1.9	0.0 \pm 0.0	70.0 \pm 13.0
real-data-E	0.0 \pm 0.0	8.0 \pm 3.0	0.0 \pm 0.0	21.3 \pm 8.0	0.0 \pm 0.0	32.7 \pm 9.5
Average	0.1	5.0	5.2	22.3	8.2	45.7

Table 8: **Comparison of algorithm performance on error metrics.**

Algorithm	Minimum Error \downarrow	Maximum Error \downarrow	Mean Error \downarrow
FORL-DCM	0.02	2.40	0.87 \pm 0.60
FORL-MAX	0.01	9.33	2.05 \pm 1.74
DQL	2.26	11.30	5.51 \pm 2.13
FORL-DM (<i>no past offsets</i>)	0.01	9.94	3.68 \pm 2.25
DQL+LAG- \bar{s}	0.04	6.28	1.76 \pm 1.13
DQL+LAG- \tilde{s}	0.05	6.56	1.87 \pm 1.19
DMBP+LAG	0.03	6.28	1.69 \pm 1.11

in antmaze-medium-diverse, it significantly underperforms in cube-single-play (Table 7). Moreover, it requires bandwidth selection and a fallback mechanism to handle numerical instability, which highlights the practical advantage of DCM.

FORL (MAX), also referred to as MAX for brevity, can fail when the forecast mean of $D_{timeseries}$ is biased, misleading it to select a candidate from a geometrically distant mode that appears more likely under an inaccurate forecast. In contrast DCM, succeeds because its state estimation is not dependent on the forecast’s mean, but on a non-parametric search for the forecast sample with the highest score (minimum dimension-wise distance). Hence, DCM’s prediction error is governed by the accuracy of the forecast sample in $D_{timeseries}$ with the best score. Empirically, this yields lower maximum and mean errors compared to MAX. The timeseries forecaster can generate a large set of samples that can be systematically biased, which is why we observe that the DQL+LAG- \bar{s} and DQL+LAG- \tilde{s} also have high maximum prediction error in Table 8. While for this specific setting in Fig. 16, FORL (MAX) and FORL-DM are close to FORL (DCM), although worse, we observe that across the test episodes, FORL (DCM) outperforms FORL (MAX) and FORL-DM in terms of maximum and mean error, demonstrating stability.

Table 9: **Normalized scores (mean \pm std.) for DCM candidate selection and the baselines.** Bold are the best values, and those not significantly different ($p > 0.05$, Welch’s t-test).

maze2d-medium	DM-FS- \bar{s}	DM-FS- \tilde{s}	FORL (MAX)	FORL(KDE)	FORL(DCM)
real-data-A	40.6 \pm 9.6	73.7 \pm 8.4	41.2 \pm 8.2	49.7 \pm 5.8	63.3 \pm 6.7
real-data-B	59.8 \pm 16.9	59.3 \pm 20.0	58.9 \pm 14.1	96.2 \pm 14.0	66.5 \pm 18.2
real-data-C	64.9 \pm 17.0	67.8 \pm 17.7	66.1 \pm 16.4	94.9 \pm 13.8	86.3 \pm 15.7
real-data-D	45.1 \pm 21.6	45.0 \pm 19.5	44.4 \pm 21.6	86.9 \pm 14.5	103.4 \pm 11.9
real-data-E	12.5 \pm 6.3	20.8 \pm 7.2	11.8 \pm 5.5	49.3 \pm 16.5	51.2 \pm 13.7
Average	44.6	53.3	44.5	75.4	74.1
maze2d-large					
real-data-A	11.9 \pm 5.5	20.8 \pm 6.2	11.1 \pm 2.3	6.6 \pm 2.2	42.9 \pm 4.1
real-data-B	27.9 \pm 14.7	25.1 \pm 11.7	28.3 \pm 7.1	20.9 \pm 7.2	34.9 \pm 9.2
real-data-C	34.6 \pm 6.8	32.4 \pm 5.8	34.6 \pm 13.6	36.0 \pm 7.3	45.6 \pm 4.1
real-data-D	16.4 \pm 12.0	15.5 \pm 9.0	18.4 \pm 9.9	11.8 \pm 3.2	58.4 \pm 6.5
real-data-E	8.4 \pm 5.0	7.9 \pm 3.9	9.2 \pm 6.1	5.7 \pm 5.1	12.0 \pm 9.9
Average	19.8	20.3	20.3	16.2	38.8
antmaze-umaze-diverse					
real-data-A	56.0 \pm 13.3	58.7 \pm 7.4	59.7 \pm 9.7	80.3 \pm 4.1	65.3 \pm 8.7
real-data-B	69.2 \pm 11.3	76.7 \pm 11.3	65.0 \pm 10.5	82.5 \pm 8.0	74.2 \pm 10.8
real-data-C	72.1 \pm 5.4	75.8 \pm 4.8	76.2 \pm 5.4	67.9 \pm 7.9	78.8 \pm 8.5
real-data-D	65.0 \pm 11.3	61.7 \pm 15.1	63.3 \pm 6.8	85.0 \pm 4.8	75.8 \pm 8.0
real-data-E	76.7 \pm 16.2	74.7 \pm 18.3	72.0 \pm 15.0	75.3 \pm 8.0	81.3 \pm 6.9
Average	67.8	69.5	67.2	78.2	75.1
antmaze-medium-diverse					
real-data-A	39.0 \pm 9.5	27.3 \pm 7.5	36.0 \pm 4.8	62.7 \pm 6.3	44.0 \pm 7.9
real-data-B	34.2 \pm 9.0	35.8 \pm 8.1	36.7 \pm 7.5	59.2 \pm 8.0	55.8 \pm 7.0
real-data-C	36.2 \pm 2.8	34.6 \pm 2.4	37.1 \pm 3.7	49.2 \pm 10.1	52.9 \pm 9.5
real-data-D	25.0 \pm 6.6	17.5 \pm 3.5	37.5 \pm 6.6	77.5 \pm 8.6	64.2 \pm 8.6
real-data-E	28.7 \pm 3.0	25.3 \pm 5.1	26.7 \pm 7.1	36.7 \pm 5.8	26.7 \pm 4.7
Average	32.6	28.1	34.8	57.1	48.7
antmaze-large-diverse					
real-data-A	25.0 \pm 7.9	21.0 \pm 3.5	21.7 \pm 7.9	21.7 \pm 8.3	34.3 \pm 5.7
real-data-B	25.0 \pm 5.1	30.0 \pm 7.5	20.0 \pm 6.8	47.5 \pm 15.2	46.7 \pm 11.9
real-data-C	25.8 \pm 4.6	21.7 \pm 2.4	23.8 \pm 6.4	40.0 \pm 7.6	33.8 \pm 6.8
real-data-D	14.2 \pm 7.0	15.8 \pm 5.4	21.7 \pm 7.5	35.0 \pm 14.3	46.7 \pm 12.6
real-data-E	21.3 \pm 8.4	22.0 \pm 7.7	20.7 \pm 4.9	8.0 \pm 3.0	11.3 \pm 7.3
Average	22.3	22.1	21.6	30.4	34.6

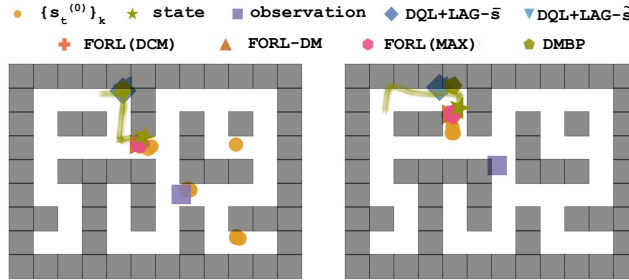


Figure 16: **Illustrations of states, observations, diffusion model predictions $\{s_t^{(0)}\}_k$, and predicted states from FORL (DCM), FORL-DM, DQL+LAG- \bar{s} , DQL+LAG- \tilde{s} , FORL (MAX), DMBP+LAG are shown.** These visualizations are from the same setting presented in Fig. 12. Maximum, minimum, and mean prediction errors across episodes for this task are provided in Table 8.

Table 10: **Intra-episode non-stationarity results with $f = 50$.** We compare methods with access to past offsets (DQL+LAG- \bar{s} vs. FORL) and without (DQL vs. FORL-DM).

maze2d-medium	DQL	FORL-DM	DQL+LAG- \bar{s}	FORL
real-data-A	31.6 ± 1.6	55.7 ± 8.7	29.7 ± 9.2	17.8 ± 4.4
real-data-B	-4.7 ± 0.2	42.2 ± 9.3	63.0 ± 9.2	100.1 ± 8.5
real-data-C	-4.7 ± 0.2	39.2 ± 7.2	88.4 ± 9.4	81.0 ± 8.3
real-data-D	25.9 ± 5.3	37.0 ± 8.4	43.1 ± 8.1	101.0 ± 7.1
real-data-E	-4.7 ± 0.2	57.0 ± 10.2	5.8 ± 2.2	66.7 ± 8.3
Average	8.7	46.2	46.0	73.3
antmaze-umaze-diverse				
real-data-A	51.0 ± 7.4	47.2 ± 10.6	70.6 ± 14.5	78.2 ± 8.0
real-data-B	63.8 ± 10.2	51.2 ± 10.3	26.0 ± 16.8	61.4 ± 9.7
real-data-C	61.0 ± 9.3	53.0 ± 6.6	91.2 ± 2.5	89.0 ± 5.1
real-data-D	17.6 ± 5.9	53.8 ± 5.7	78.0 ± 4.4	90.0 ± 2.9
real-data-E	0.2 ± 0.4	51.0 ± 11.6	80.6 ± 9.7	85.6 ± 5.5
Average	38.7	51.2	69.3	80.8
antmaze-medium-diverse				
real-data-A	42.8 ± 6.9	7.2 ± 1.8	50.4 ± 2.9	54.8 ± 5.2
real-data-B	5.0 ± 3.1	37.4 ± 3.8	41.2 ± 4.8	47.2 ± 4.6
real-data-C	12.0 ± 5.1	26.8 ± 2.4	71.2 ± 2.9	61.4 ± 4.5
real-data-D	24.0 ± 4.7	30.4 ± 2.9	61.6 ± 5.0	70.2 ± 6.6
real-data-E	2.2 ± 2.3	21.0 ± 3.3	33.0 ± 5.0	37.0 ± 3.4
Average	17.2	24.6	51.5	54.1
antmaze-large-diverse				
real-data-A	13.0 ± 5.5	5.8 ± 2.6	16.0 ± 3.8	27.4 ± 3.6
real-data-B	1.2 ± 0.8	11.4 ± 4.9	19.4 ± 4.6	50.2 ± 9.7
real-data-C	4.8 ± 2.9	7.2 ± 0.8	31.8 ± 4.4	48.6 ± 4.3
real-data-D	4.6 ± 1.3	11.0 ± 2.5	25.2 ± 2.9	48.2 ± 6.2
real-data-E	2.4 ± 1.5	13.6 ± 4.8	12.8 ± 3.4	13.4 ± 2.2
Average	5.2	9.8	21.0	37.6

H.1 Sensitivity to Diffusion-generated Sample Size

MAX uses candidate states predicted by the diffusion model in the FORL framework and Lag-Llama but uses maximum likelihood instead of DCM. Given the multimodal nature of the candidate state distributions, we conduct a sensitivity analysis on the number of denoiser samples, a shared hyperparameter for both MAX and FORL. We report results averaged over 5 random seeds across 25 tasks (antmaze and maze2d with real-data-A, B, C, D, E). The results in Fig. 17 indicate that our diffusion model’s performance remains consistent across varying sample sizes, demonstrating robustness to the number of candidate states generated. Notably DMBP algorithm uses 50 denoiser samples.

I Zero-shot Foundation Model and Time-Series Datasets

We extract the first two univariate series from five time-series datasets: real-data-A (australian-electricity-demand) [73], real-data-B (electricity)[74], real-data-C (electricity-hourly) [73, 74], real-data-D (electricity-nips) [74, 75] and real-data-E (exchange-rate²) [76], [73] all accessed via GluonTS [22, 77]. Figure 5 presents the ground truth, forecast mean, and standard deviation from Lag-Llama [10] for the first series of real-data-A and real-data-D; forecasts for the remaining series and domains are provided in Figure 18.

²<https://github.com/laiguokun/multivariate-time-series-data>

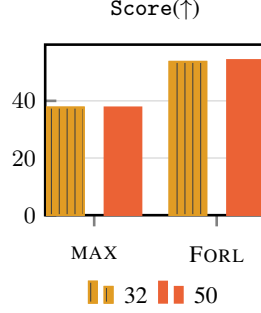


Figure 17: **Average normalized scores over 25 experiments with diffusion-generated sample sizes of 32 and 50, each conducted with 5 random seeds.** The results indicate that the diffusion model’s performance remains consistent across varying sample sizes, demonstrating robustness to the number of candidate states generated.

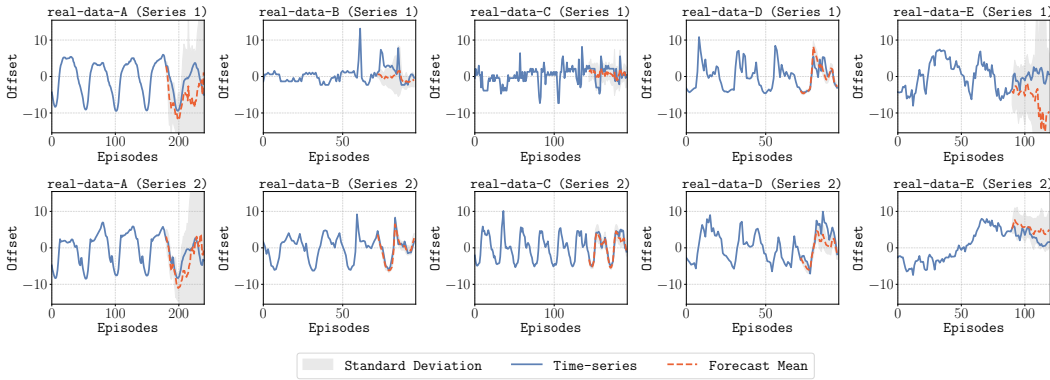


Figure 18: Zero-shot forecasting results with Lag-Llama [10] for first 2 time-series in univariate time-series datasets: `real-data-A` (Australian-electricity-demand), `real-data-E` (Exchange Rate), `real-data-B` (Electricity), `real-data-C` (Electricity Hourly), `real-data-D` (Electricity Nips).

We aim to capture a broad spectrum of scenarios for a comprehensive evaluation. For instance, the `electricity-hourly` dataset provides hourly electricity usage data from various consumers, while the `australian-electricity-demand` dataset offers 30-minute interval records of electricity demand across different Australian states. The `exchange-rate` dataset, on the other hand, includes daily exchange rates of multiple currencies, including those of Australia, the United Kingdom, Canada, Switzerland, China, Japan, New Zealand, and Singapore.

To effectively represent diverse offset patterns in multiple directions, we apply feature scaling to the time-series data using a normalization $x'_c = \frac{x - \bar{x}}{\max(x) - \min(x)}$ where sample mean \bar{x} , $\min(x)$ and $\max(x)$ are computed from the available data up to the context length. Furthermore, we scale these values using the minimum and maximum state values observed in the offline RL dataset [15] for navigation and minimum and maximum state values of the initial state distribution at test time for manipulation [15], ensuring diverse observation spaces that can accurately represent a wide range of scenarios. We group our results in terms of time-series datasets in Table 13.

I.1 Sensitivity of FORL to Forecasting Errors

To analyze the sensitivity of FORL to forecasting errors, we compare its performance against `DQL+LAG- \bar{s}` , which only uses the forecaster’s predictions. Table 11 presents the average prediction error (\downarrow) across all datasets in `antmaze` and `maze2d` environments with 5 seeds.

In all datasets, FORL outperforms the `DQL+LAG- \bar{s}` baseline. FORL achieves its greatest impact on moderately challenging forecasts (a 56.5% error reduction on `real-data-D`). Its behavior at the extremes further demonstrates its robustness:

Table 11: **Sensitivity analysis of FORL to forecasting errors.** We compare the average prediction error (\downarrow) of our method against the DQL+LAG- \bar{s} baseline, which uses only the forecaster’s predictions. The analysis is presented across five time-series datasets. Error reduction percentages are calculated from full-precision values before rounding.

Dataset	DQL+LAG- \bar{s} (\downarrow)	FORL (\downarrow)	Error Reduction(\uparrow)
real-data-A	4.56	3.32	27.0%
real-data-B	3.66	2.29	37.4%
real-data-C	3.0	2.69	10.2%
real-data-D	4.29	1.87	56.5%
real-data-E	5.45	5.21	4.3%

- FORL still refines the best forecast by 10.2% (real-data-C)
- FORL improves the worst forecast by 4.3% (real-data-E).

I.2 State Prediction Accuracy

To evaluate the state-prediction accuracy of our FORL framework, we compare it against DQL+LAG- \bar{s} . For each method, we report the mean ℓ_2 error between the true state s_t and the predicted state \tilde{s}_t obtained during evaluation for a diffusion-generated sample size of 32.

In the resulting average prediction error table in Table 12:

- Each **row** corresponds to the state estimation algorithm used at test time to generate states \tilde{s}_t , which are then provided to the policy to select actions.
- Each **column** corresponds to a method whose state estimates are evaluated on that same rollout.

The entry at row i , column j is the mean ℓ_2 error when method m_i is used in the environment, but predictions are produced by method m_j . When $i = j$, this entry measures the self-prediction error of each method; when $i \neq j$, it measures the error under an alternate method.

Across all method pairs, FORL achieves lower mean ℓ_2 errors, even in off-diagonal evaluations, demonstrating its superior state-prediction performance compared to DQL+LAG- \bar{s} . These findings are consistent with the normalized environment scores in Table 1.

Table 12: **Comparison of prediction errors (\downarrow).** We present state prediction accuracy for the proposed FORL framework with the baselines across 5 random seeds.

maze2d-medium	DQL+LAG- \bar{s}	FORL
DQL+LAG- \bar{s}	1.68 ± 0.46	1.35 ± 0.48
FORL	1.39 ± 0.49	1.25 ± 0.43
maze2d-large	DQL+LAG- \bar{s}	FORL
DQL+LAG- \bar{s}	2.37 ± 0.5	1.63 ± 0.57
FORL	1.91 ± 0.44	1.39 ± 0.62
antmaze-large-diverse	DQL+LAG- \bar{s}	FORL
DQL+LAG- \bar{s}	8.07 ± 1.83	5.33 ± 2.17
FORL	7.16 ± 1.71	5.89 ± 2.96
antmaze-medium-diverse	DQL+LAG- \bar{s}	FORL
DQL+LAG- \bar{s}	5.33 ± 1.15	4.75 ± 1.98
FORL	4.94 ± 1.17	4.74 ± 1.63
antmaze-umaze-diverse	DQL+LAG- \bar{s}	FORL
DQL+LAG- \bar{s}	3.51 ± 0.53	2.04 ± 0.47
FORL	3.27 ± 0.61	2.31 ± 0.51

Table 13: **Normalized scores (mean \pm std.) for FORL framework and the baselines grouped by time-series.** Bold are the best values, and those not significantly different ($p > 0.05$, Welch’s t-test).

real-data-A	DQL	DQL+LAG- \bar{s}	DMBP+LAG	FORL (ours)
maze2d-medium	30.2 \pm 6.5	30.2 \pm 8.6	25.1 \pm 9.8	63.3 \pm 6.7
maze2d-large	16.2 \pm 5.5	2.4 \pm 1.1	4.2 \pm 5.8	42.9 \pm 4.1
antmaze-umaze-diverse	22.7 \pm 3.0	41.0 \pm 5.2	45.7 \pm 4.8	65.3 \pm 8.7
antmaze-medium-diverse	31.0 \pm 6.5	40.0 \pm 5.7	39.7 \pm 4.0	44.0 \pm 7.9
antmaze-large-diverse	11.0 \pm 1.9	11.3 \pm 4.9	9.0 \pm 4.5	34.3 \pm 5.7
kitchen-complete	16.6 \pm 1.4	7.2 \pm 1.9	8.7 \pm 1.3	12.0 \pm 3.9
real-data-B				
maze2d-medium	14.1 \pm 12.1	53.4 \pm 14.6	41.2 \pm 21.1	66.5 \pm 18.2
maze2d-large	-0.5 \pm 2.9	5.5 \pm 9.0	15.0 \pm 14.6	34.9 \pm 9.2
antmaze-umaze-diverse	24.2 \pm 3.5	48.3 \pm 7.0	62.5 \pm 13.2	74.2 \pm 10.8
antmaze-medium-diverse	23.3 \pm 4.8	48.3 \pm 4.8	43.3 \pm 16.0	55.8 \pm 7.0
antmaze-large-diverse	5.8 \pm 4.8	9.2 \pm 4.6	8.3 \pm 2.9	46.7 \pm 11.9
kitchen-complete	12.9 \pm 4.1	32.7 \pm 6.5	20.0 \pm 3.1	33.1 \pm 5.6
real-data-C				
maze2d-medium	-2.3 \pm 3.3	56.7 \pm 18.5	56.9 \pm 18.4	86.3 \pm 15.7
maze2d-large	0.9 \pm 1.7	16.6 \pm 7.5	26.8 \pm 8.4	45.6 \pm 4.1
antmaze-umaze-diverse	21.7 \pm 3.5	50.4 \pm 8.3	60.4 \pm 3.9	78.8 \pm 8.5
antmaze-medium-diverse	10.0 \pm 2.3	48.3 \pm 3.4	49.6 \pm 3.7	52.9 \pm 9.5
antmaze-large-diverse	5.4 \pm 2.4	22.1 \pm 5.6	17.9 \pm 3.8	33.8 \pm 6.8
kitchen-complete	13.4 \pm 1.7	23.9 \pm 6.6	20.5 \pm 3.3	23.9 \pm 6.0
real-data-D				
maze2d-medium	4.7 \pm 5.0	36.9 \pm 16.3	38.5 \pm 14.2	103.4 \pm 11.9
maze2d-large	3.0 \pm 6.6	8.6 \pm 3.2	13.4 \pm 4.1	58.4 \pm 6.5
antmaze-umaze-diverse	5.8 \pm 2.3	26.7 \pm 6.3	29.2 \pm 5.9	75.8 \pm 8.0
antmaze-medium-diverse	11.7 \pm 5.4	46.7 \pm 7.5	41.7 \pm 6.6	64.2 \pm 8.6
antmaze-large-diverse	2.5 \pm 2.3	14.2 \pm 3.7	14.2 \pm 6.3	46.7 \pm 12.6
kitchen-complete	7.5 \pm 2.5	24.0 \pm 9.2	28.1 \pm 8.1	27.1 \pm 10.1
real-data-E				
maze2d-medium	3.5 \pm 8.8	8.7 \pm 6.0	11.4 \pm 2.8	51.2 \pm 13.7
maze2d-large	-2.1 \pm 0.4	2.6 \pm 3.4	0.9 \pm 3.7	12.0 \pm 9.9
antmaze-umaze-diverse	6.0 \pm 6.8	58.0 \pm 16.6	59.3 \pm 7.6	81.3 \pm 6.9
antmaze-medium-diverse	18.7 \pm 4.5	27.3 \pm 8.6	26.0 \pm 5.5	26.7 \pm 4.7
antmaze-large-diverse	5.3 \pm 3.8	3.3 \pm 2.4	3.3 \pm 0.0	11.3 \pm 7.3
kitchen-complete	18.5 \pm 6.0	2.8 \pm 2.1	6.2 \pm 1.7	10.3 \pm 3.0

J Preliminary Results for Affine Transformation with Uniform Scaling and Bias

We use the fourth series in each time-series domain to perform isotropic scaling for the dimensions affected by non-stationarity using a scaling factor of $\beta = 0.5$, with bias coming from the first two series, respectively. We apply feature scaling to time-series data with $x'_c = 1 - \beta + \beta \cdot \exp\left(\frac{x - \bar{x}}{2 \cdot (\max(x) - \min(x))}\right)$. The offset scaling for the bias uses $\alpha = 1$, which is the standard value in our experiments. As in the other ablations with scaling offsets, we use the DQL policy. Table 14 shows that FORL outperforms the baselines under this transformation. A large-scale analysis of more general transformations is left for future work.

Table 14: **Performance under affine observation shifts.** Normalized scores in maze2d-large with time-varying uniform scaling and bias.

maze2d-large	DQL	DQL+LAG- \bar{s}	FORL (ours)
real-data-A	5.9	6.1	39.7
real-data-B	2.4	1.6	13.8
real-data-C	2.2	22.2	32.9
real-data-D	0.7	10.7	56.1
real-data-E	-2.0	-2.3	27.5
Average	1.8	7.7	34.0

K Offline Reinforcement Learning Environments

K.1 D4RL

We use the standard D4RL [15] offline RL environments [15] with no modifications during training, namely `antmaze-medium-diverse`, `maze2d-medium`, `antmaze-large-diverse`, `maze2d-large`, and `antmaze-umaze-diverse`, where initial states are randomized both in the evaluation environment and in the offline dataset. Fig. 19 illustrates the environments used from the D4RL benchmark, `kitchen-complete`, `antmaze-large-diverse`, `antmaze-medium-diverse`, `antmaze-umaze-diverse`. The `maze2d-large` and `maze2d-medium` environments share the same maze configurations as `antmaze-large-diverse` and `antmaze-medium-diverse`, respectively.

For manipulation tasks, we train on the standard `kitchen-complete` environment. We sample the base joint angles from $U([-1.5, 0.17])$ and the shoulder-joint angles from $U([-1.78, -1.16])$ which are set based on the minimum and maximum state space dimension intervals in the offline RL dataset to evaluate partial identifiability at test-time. The offsets affect the state dimensions associated with the base and shoulder joint angles.

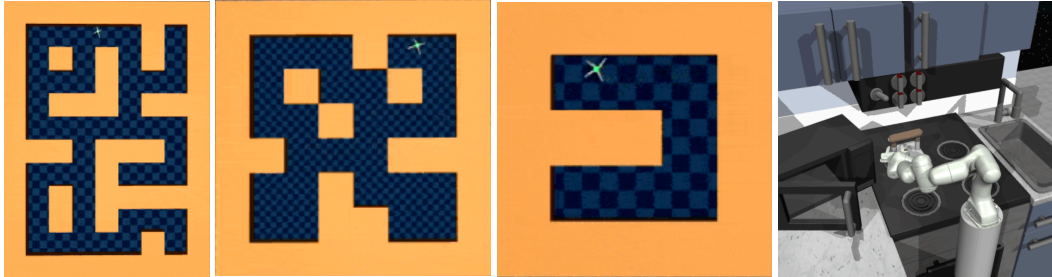


Figure 19: `antmaze-large`, `antmaze-medium`, `antmaze-umaze (-v1)` and `kitchen-complete` environments in D4RL benchmark [15].

K.2 OGBench

OGBench benchmark [21] contains both standard and goal-conditioned offline reinforcement learning tasks. To induce non-stationarity at test time, we follow the procedure from our D4RL experiments and use time-series data from GluonTS [22, 77]. For all tasks in Fig. 21, we use the default `singletask-v0` variant. We report results using the FQL algorithm [23] with its officially recommended hyperparameters. For the `antmaze-large-navigate` environment, we use the first two time series from the GluonTS `real-data-A,B,C,D,E` datasets and apply an offset scaling factor of $\alpha = 0.5$. For `cube-single-play`, we apply offsets to the first 17 observation dimensions, which include all joint positions, joint velocities, and end effector variables (position and yaw), using the first 17 time series from each of the GluonTS `real-data-A,B,C,D,E` datasets. Because the `real-data-A` dataset only has five time series, we cycle through them repeatedly until all 17 dimensions are covered. Across all `cube-single-play` experiments, we use an offset scaling factor of $\alpha = 0.25$.

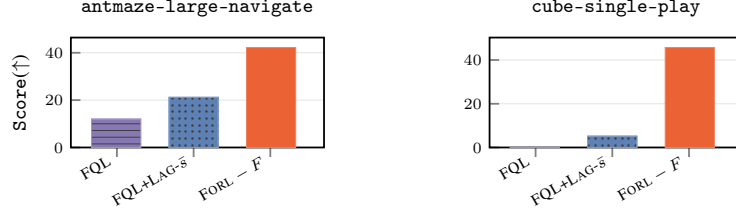


Figure 20: Average normalized scores of FORL (ours) and baselines for OGBench



Figure 21: cube-single-play and antmaze-large-navigate environments in OGBench benchmark [21].

L Implementation Details

During training, we use the original offline RL dataset **without offsets**. At test-time, the offsets affect the first two state dimensions, where each offset sequence is drawn from the first two univariate time-series from diverse datasets. The agent’s policy receives only the offset-corrupted observations, with no direct access to the true underlying states throughout P episodes. The time-series forecasting model, given the past C ground-truth offsets $(b^{j-C}, \dots, b^{j-1})$, predicts the future offsets (b^j, \dots, b^{j+P}) during testing. FORL leverages these predictions and in-episode experience to dynamically adapt to unknown external perturbations. All experiments use 5 random seeds, except for (i) the preliminary affine-transformation results (Section J) and (ii) the focused error analysis across all evaluation episodes for the task shown in Fig. 16 with results reported in Table 8.

We select the hyperparameters in Table 20 based on the validation loss of the FORL diffusion model in D4RL and OGBench standard offline RL datasets. The validation loss is computed using the DM loss function in Eq. 4. Hyperparameter optimization was conducted using a grid search, with the following ranges for maze2d and antmaze: diffusion timesteps $N = \{10, 20\}$, number of hidden layers following the Temporal Unet model $\#layers = \{1, 2, 3\}$, window size $w = \{128, 256\}$, and learning rate $lr = \{0.0004, 0.0006, 0.0009\}$. For the kitchen-complete and cube-single-play embedding dimension $= \{64, 128\}$, learning rates $lr = \{0.0004, 0.0009\}$ and $w = \{32, 64\}$ are used for the grid search.

The architecture of our FORL Model is a noise prediction conditional TemporalUnet diffusion model [3, 39, 78]. Different from the architecture used in [3], we concatenate each element in $\tau_{(t,w)}$ with $s_t^{(n)}$ and feed it to our model without additional encoders, using the diffusion timestep embedding in the Residual Temporal Blocks. For the TemporalUnet architecture, we concatenate the Unet model output with the time-embedding before feeding it to fully connected layers, particularly in the antmaze environments due to the large input size. The set of hyperparameters is provided in Table 20. Although the FORL conditional diffusion model is specifically utilized for time-dependent offsets in the first two dimensions of the state vector, it is trained for general-purpose state prediction, enabling it to predict all dimensions of the state in maze2d, antmaze, and OGBench environments. This approach is taken because we do not assume prior knowledge of the evaluation environment.

The method for setting seeds involves a function that initializes the seed across all relevant libraries (PyTorch, CUDA, NumPy, Gym Environment, and Python’s random module) to ensure the replicabil-

ity of results. We use the open source implementation of DMBP³ with the suggested hyperparameters [56], and the pretrained Lag-Llama⁴ model[10].

M Experiments compute resources

Experiments were primarily conducted on an HPC cluster with NVIDIA A100 GPUs (40GB HBM2, PCIe 4.0/NVLink interconnect) and AMD EPYC 7302 CPUs (32 cores, 1TB RAM, 3TB local SSD), as well as on a workstation with an NVIDIA GeForce RTX 4090 (24GB GDDR6X), 128GB RAM, and a 2TB PCIe 4.0 NVMe SSD. A small portion of the experiments also ran on a cluster equipped with 4x NVIDIA V100 GPUs (16GB NVLink), 2x Intel Xeon Gold 6248R CPUs, and 384GB RAM. The total compute for published results is approximately 7,300 GPU-hours; additional failed and preliminary runs total approximately 1,500 GPU-hours.

Table 15: Hyperparameters for DQL [14, 79, 80] across kitchen-complete, maze2d, and antmaze environments.

Hyperparameters					
Maximum Timesteps	1 000 000				
γ	0.99				
τ	0.005				
Learning rate decay	true				
T	10				
β Schedule	vp				
Learning rate	3×10^{-4}				
α	0.2				
Batch Size	256				
Hidden Size	256				
Reward tune	no				
Normalize	false				
Optimizer	Adam[81]				
		kitchen-complete	maze2d	antmaze	
gn	10.0		umaze-diverse: 3.0	umaze-diverse:	3.0
			medium-diverse: 1.0	medium-diverse:	1.0
			large-diverse: 7.0	large-diverse:	7.0
η	0.005		umaze-diverse: 2.0	umaze-diverse:	2.0
			medium-diverse: 3.0	medium-diverse:	3.0
			large-diverse: 3.5	large-diverse:	3.5
MaxQ Backup	false		true		true

Table 16: Hyperparameters for Implicit Q-Learning (IQL) [26, 63, 82, 83] across maze2d, and antmaze environments.

Hyperparameters	Value
Batch Size	256
Discount (γ)	0.99
Target Network Update (τ)	0.005
maze2d	$\beta = 3.0$ $\tau_{\text{IQL}} = 0.7$ Normalize Rewards = false
antmaze	$\beta = 10.0$ $\tau_{\text{IQL}} = 0.9$ Normalize Rewards = true

³<https://github.com/zhyang2226/DMBP/tree/main>

⁴<https://github.com/time-series-foundation-models/Lag-Llama>

Table 17: Hyperparameters for Flow Q-Learning (FQL) [23, 84] for cube-single-play and antmaze-large-navigate.

Hyperparameters	Value
Batch Size	256
Learning Rate	0.0003
Discount factor (γ)	0.99
Target network smoothing coefficient (τ)	0.005
BC Coefficient (α)	10.0
Flow Steps	10
Actor Hidden Dimensions	(512, 512, 512, 512)
Value Hidden Dimensions	(512, 512, 512, 512)
antmaze-large-navigate	BC Coefficient (α) = 10.0
cube-single-play	BC Coefficient (α) = 300.0

Table 18: Hyperparameters for TD3BC [59, 80, 85] across kitchen-complete, maze2d, and antmaze environments.

Hyperparameters	Value
Maximum Timesteps	1 000 000
Exploration noise	0.1
Batch Size	256
Discount factor	0.99
τ	0.005
Policy Noise	0.2
Policy Noise Clipping	0.5
Policy update frequency	2
α	2.5
Normalize	true
Optimizer	Adam[81]

Table 19: Hyperparameters for RORL [25, 80, 86] in maze2d environments.

Hyperparameters	
γ	0.99
soft τ	0.005
Q Learning Rate	3×10^{-4}
Policy Learning Rate	3×10^{-4}
α	1.0
Auto-tune entropy	true
MaxQ Backup	false
Deterministic Backup	false
η	-1
Batch Size	256
Hidden Size	256
Target Update Interval	1
τ	0.2
Normalize	false
n sample	20
β_Q	0.0001
β_P	1.0
ϵ_{ood}	0.01
Maximum Timesteps	3 000 000
Optimizer	Adam[81]
	maze2d
β_{OOD}	0.5
ϵ_Q	0.01
ϵ_P	0.03
λ_{max}	1.0
λ_{min}	0.5
λ_{decay}	10^{-6}

Table 20: Hyperparameters for FORL across kitchen-complete, maze2d, antmaze, antmaze-large-navigate, cube-single-play environments.

Hyperparameters					
Batch Size	128				
Hidden Size	128				
# denoiser samples	50				
Optimizer	Adam[81]				
Maximum Timesteps	300 000				
	kitchen-complete	antmaze	maze2d	antmaze-large-navigate	cube-single-play
Embedding Dimension	128	64	64	64	128
w	32	256	128	256	64
Learning rate	4×10^{-4}	4×10^{-4}	9×10^{-4}	4×10^{-4}	9×10^{-4}
Observation Scale	1	1	100	1	1
Time Concatenation	true	true	false	true	true
# middle hidden layers	1	1	large: 1 medium: 3	1	1
N	10	10	large: 10 medium: 20	20	20

N Licenses for Existing Assets and Libraries

N.1 Existing Assets

- The **D4RL**[15], including the Franka Kitchen tasks, are distributed under the Creative Commons Attribution 4.0 (data) and Apache 2.0 (code) licenses as in <https://github.com/Farama-Foundation/D4RL>.
- **MuJoCo**[87] is released under the Apache 2.0 license as indicated in <https://github.com/google-deepmind/mujoco/blob/main/LICENSE>.
- **Gymnasium** (formerly OpenAI Gym) is distributed under the MIT license as indicated in <https://github.com/Farama-Foundation/Gymnasium/blob/main/LICENSE>.
- The real-data-B dataset (UCI “Electricity Load Diagrams 2011-2014”)[88] is distributed under the Creative Commons Attribution 4.0 International license as indicated in <https://archive.ics.uci.edu/ml/datasets/electricityloaddiagrams20112014>.
- The real-data-D and real-data-C variants are derived from the same UCI data and inherit the CC-BY-4.0 license.
- The real-data-A dataset⁵ [73] is distributed under the Creative Commons Attribution 4.0 International license as indicated in <https://doi.org/10.5281/zenodo.4659727>.
- The real-data-E dataset introduced by Lai et al. [76] with publicly available financial data; no explicit license is provided in the original repository (<https://github.com/laiguokun/multivariate-time-series-data>), and it is used in [73], which distributes its datasets under the Creative Commons Attribution 4.0 International license.

N.2 Libraries

The libraries used in our experiments are:

1. `diffuser` uses the MIT License.⁶
2. `einops` uses the MIT License.⁷
3. `imageio` uses the BSD 2-Clause License.⁸
4. `loguru` uses the MIT License.⁹
5. `matplotlib` [89] uses a PSF-based license.¹⁰

⁵Half-hourly demand for five Australian states

⁶<https://github.com/jannerm/diffuser/blob/master/LICENSE>

⁷<https://github.com/arogozhnikov/einops/blob/main/LICENSE>

⁸<https://github.com/imageio/imageio/blob/master/LICENSE>

⁹<https://github.com/Delgan/loguru/blob/master/LICENSE>

¹⁰<https://github.com/matplotlib/matplotlib/blob/master/LICENSE/LICENSE>

6. `mujoco_py` uses the MIT License.¹¹
7. `numpy` uses the BSD 3-Clause License.¹²
8. `pandas` uses the BSD 3-Clause License.¹³
9. `scikit-video` uses the BSD 3-Clause License.¹⁴
10. `torch` (PyTorch)) is distributed under a permissive, BSD-style license that includes an express patent grant.¹⁵
11. `tqdm` is licensed under MIT and MPL-2.0.¹⁶
12. `ogbench` uses the MIT License.¹⁷

¹¹<https://github.com/openai/mujoco-py/blob/master/LICENSE>

¹²<https://numpy.org/doc/stable/license.html>

¹³<https://github.com/pandas-dev/pandas/blob/main/LICENSE>

¹⁴<https://github.com/scikit-video/scikit-video/blob/master/LICENSE.txt>

¹⁵<https://github.com/pytorch/pytorch/blob/main/LICENSE>

¹⁶<https://github.com/tqdm/tqdm/blob/master/LICENCE>

¹⁷<https://github.com/seohongpark/ogbench/blob/master/LICENSE>